Gesellschaft für Anlagen- und Reaktorsicherheit (GRS) mbH

Investigations on Self-Sealing of Indurated Clay

Final Report

GRS - 230

Gesellschaft für Anlagen- und Reaktorsicherheit (GRS) mbH

Investigations on Self-Sealing of Indurated Clay

Part of the NF-PRO Projects

Final Report

Chun-Liang Zhang
Tilmann Rothfuchs
Jürgen Dittrich
Jürgen Müller

March 2008

Remark:

This report was prepared under contract No. 02E9834 with the Bundesministerium für Wirtschaft und Technologie (BMWi) and under contract No. F16W-CT-2003-02389 with the Commission of the European Communities in the sixth framework programme for research and training in the field of nuclear energy (2002 – 2006).

The work was conducted by the Gesellschaft für Anlagen- und Reaktorsicherheit (GRS) mbH.

The authors are responsible for the content of this report.

GRS - 230
ISBN 978-3-939355-04-5

Deskriptoren:

Blockade, Endlager, EU, Gas, Geomechanik, Gestein, Grundwasser, Internationale Zusammenarbeit, Labor, Modell, Permeabilität

Foreword

Within the framework of the integrated NF-PRO project, initiation, development, and self-sealing / healing of the excavation damaged zone (EDZ) around a repository in indurated clay were investigated, including laboratory tests, field observations, and numerical modelling. GRS contributed with a comprehensive laboratory programme to WP4.3 (EDZ short term evolution) examining ventilation effects on deformation and damage of the Opalinus clay and to WP4.4 (EDZ long term evolution) providing evidence for self-sealing of both the Opalinus clay and the Callovo-Oxfordian-argillite.

Within WP4.4, various self-sealing experiments were carried out on strongly damaged clay samples by measuring the gas permeability as a function of the confining stress before and after water resaturation. All laboratory observations suggest a high self-sealing capacity of the studied clay rocks. In addition, modelling exercises were also performed. Details of the work are given in this report.

The GRS work was funded by the German Federal Ministry of Economics and Technology (BMWi) under contract No. 02E9834 and by the European Commission in the sixth framework programme for research and training in the field of nuclear energy under contract No. F16W-CT-2003-02389.

Table of Contents

1 Introduction

Clay formations are worldwide under consideration as a host rock for radioactive waste disposal because of their favourable properties, particularly the very low hydraulic conductivity, the low diffusion coefficient, and the high retention capacity for radionuclides. However, excavation of an underground repository leads to a redistribution of the rock stresses which results in fractures and cracks around the openings when the damage and failure criteria of the rock are violated. Hence the hydraulic conductivity of the excavation damaged zone (EDZ) can increase up to the point where the barrier function of the host rock with respect to radionuclide migration may be affected. Damage intensity and extent of the EDZ are mainly dependent on the mechanical properties of the rock, overburden stress, applied excavation technology, opening geometry and support. During the operation of a repository in a clay formation, intensity and extent of the EDZ increase due to the time-dependent deformation, pore pressure change, de-saturation and also chemical alteration in the surrounding rock mass. After backfilling and closing of the repository, gradual reconsolidation and sealing of the EDZ is to be expected due to the significant creep and swelling capability of plastic clay or even more brittle clay rocks as a consequence of the combined impact of

- the delayed rock deformation towards the EDZ,
- the backfill support, and
- the expansion of the fractured clay matrix by taking up water from the saturated far-field.

Sealing of the EDZ around repositories in clay formations is obviously a complex long-term hydro-mechanical process. Another important factor influencing the properties and the development of the EDZ is heat transfer from the high-level radioactive waste to the rock mass. The key processes related to the EDZ around a disposal cell in indurated clay are schematically illustrated in Figure 1.1. Long-term safety assessment for a repository requires therefore deep understanding, quantitative characterisation, and prediction of the long-term sealing process of the EDZ.

In the framework of the integrated NF-PRO project, initiation, development, and self-sealing / healing of the EDZ around a repository in indurated clay were investigated, including laboratory tests, field observations, and numerical modelling. GRS

contributed with a comprehensive laboratory programme to the NF-PRO-WP4.3 (EDZ short term evolution) examining ventilation effects on deformation and damage of the Opalinus clay and to the NF-PRO-WP4.4 (EDZ long term evolution) providing evidence for self-sealing of both the Opalinus clay and the Callovo-Oxfordian-argillite.

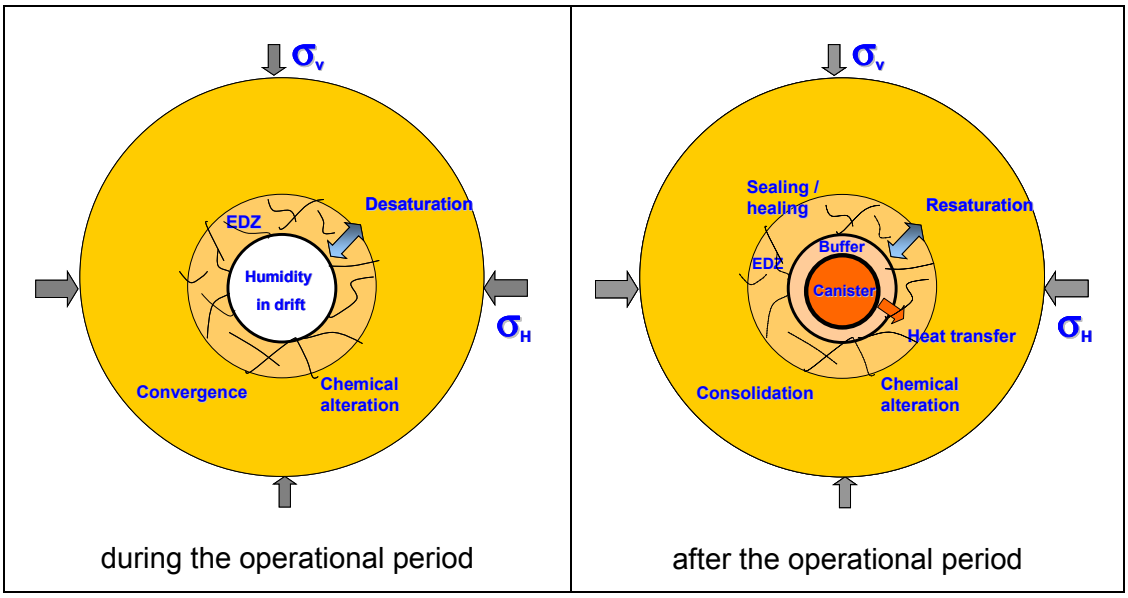

Figure 1.1 Key processes in the damaged rock zone around a disposal cell.

The main objectives of the GRS laboratory programme within the WP4.4 were

- to investigate the self-sealing potential of damaged clay samples of normal and large sizes, and
- to model laboratory large-scale damage & sealing tests to validate the suitability of the clay damage model developed by Vaunat et al. /VAU 03/04/.

The GRS work was performed under contract number 02E9834 with the German Federal Ministry of Economics and Technology (BMWi) and under contract number F16W-CT-2003-02389 with the Commission of the European Communities in the sixth framework programme for research and training in the field of nuclear energy. The project covered the time period between July 2005 and December 2007. In this report, achievements and results of the GRS work are presented.

2 Laboratory experiments

Previous experiments performed by GRS /ZHA 04-07/ suggested that indurated clay such as the Callovo-Oxfordian argillite and the Opalinus clay possess a significant creep and swelling potential. Therefore, it can be expected that fractures of an EDZ around an underground repository in clay tend to close after backfilling and sealing the repository under the combined impact of reconsolidation and rehydration.

Under consideration of relevant repository conditions, the self-sealing potential of the Callovo-Oxfordian argillite at the MHM-URL in France and the Opalinus clay at the Mont-Terri-URL in Switzerland was investigated in the GRS geotechnical laboratory. The Callovo-Oxfordian argillite contains 40-45% clay minerals, 20-30% carbonates and 20-30% quartz and feldspar /AND 05/. Mineral composition of the Opalinus clay is 45-76% clay minerals, 6-30% quartz, 6-39% calcite and 2-4% feldspars /PEA 03/. Both the Callovo-Oxfordian argillite and the Opalinus clay are indurated sedimentary rocks with significant stiffness and strength, differing from less consolidated plastic clays such as the Boom clay at the HADES-URL in Belgium.

The self-sealing potential of a clay rock can be characterised by various parameters such as closure of pre-existing cracks or decrease of permeability of the representative damaged rock mass under prevailing in-situ conditions. As a direct indicator for self-sealing, the changing permeability of damaged samples can be measured in laboratory tests. Within the GRS experimental programme, various self-sealing tests were carried out on strongly-damaged samples with measurement of changes in gas permeability due to re-compaction, and resaturation. Not only normally-sized but also large-scale and hollow cylindrical samples were tested. The tests lasted between 5 to 16 months.

2.1 Tests on normally-sized samples

2.1.1 Preparation of samples

Four samples were prepared from core MSE00953 drilled at a depth of 621 m in the Callovo-Oxfordian argillite at the MHM-URL. The core axis is perpendicular to the bedding plane. After unpacking from the confining cell, the core of 300 mm length broke up in three parts along the bedding planes. They were prepared to sample sizes

of a diameter of 86.5 mm and different lengths from 43 to 86 mm, as given in Table 1. The mean bulk density amounted to 2.45 g/cm^3. From another core (MSE00837) drilled from the same borehole and subject to the same confinement as core MSE00953, the following petrophysical properties were determined: a grain density of 2.70 g/cm^3, a dry density of 2.32 g/cm^3, a porosity of 14.1%, and a water content of 4.55%. The degree of water saturation was derived to be 75%.

Three samples, MSE00953-2/-3/-4, were damaged in a triaxial cell by increasing axial stress at a lateral stress of 3.1 MPa. Figure 2.1 shows the measured deviatoric stress and volumetric strain over axial strain. It is obvious that the samples were loaded above their peak strengths which lay in the range between 31.5 and 34.5 MPa. The volumetric strain curves indicate that the samples were first compacted with increasing deviatoric stress until onset of dilatancy. The dilatancy point is close to the failure strength. Some photos of the damaged samples are shown in Figure 2.2. It can clearly be seen that major fractures were aligned more horizontally with the bending planes rather than vertically with the major loading direction. As a reference, sample MSE00953-1 was tested, too, which was not artificially damaged by loading but already disturbed during sampling and preparation. The test data obtained from the damaged samples are given in Table 1.

Table 1 Characterization of damaged samples from the Callovo-Oxfordian argillite

Sample	Diameter (mm)	Length (mm)	Bulk density (g/cm^3)	Confining stress (MPa)	Failure strength (MPa)	Axial strain (%)	Volumetric dilatancy (%)
MSE00953-1	86.5	42.6	2.461	not loaded			
MSE00953-2	86.5	81.9	2.435	3.1	35.7	1.74	0.71
MSE00953-3	86.5	75.2	2.455	3.1	37.4	1.17	0.50
MSE00953-4	86.5	86.0	2.436	3.1	34.6	1.84	0.54

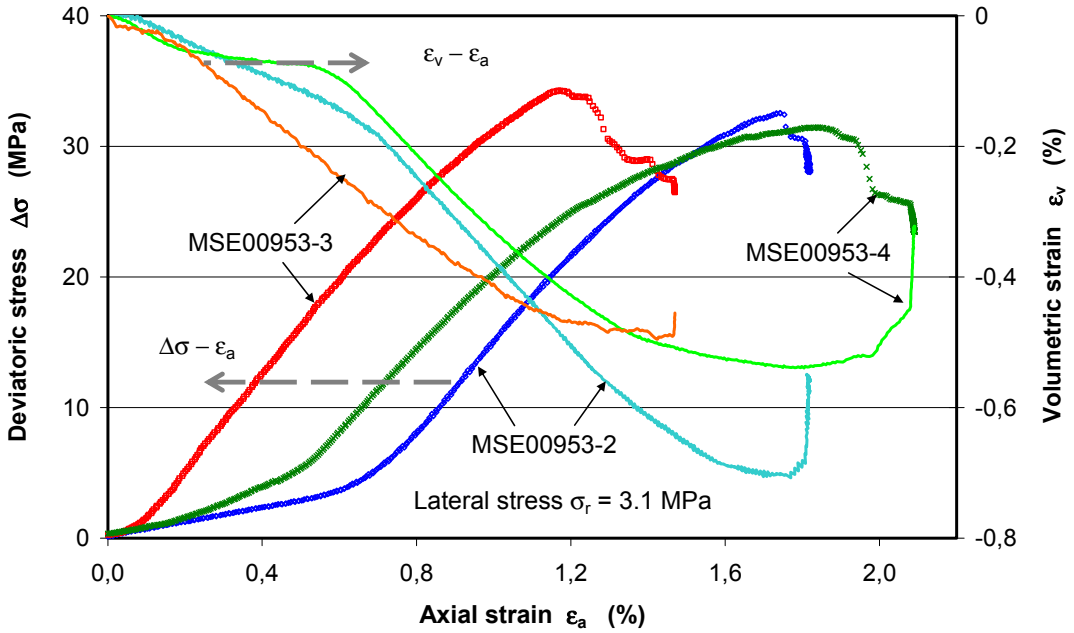

Figure 2.1 Stress / strain curves obtained by damaging the clay samples

Figure 2.2 Photos of strongly damaged samples from the Callovo-Oxfordian argillite

2.1.2 Test method

The self-sealing behaviour of the damaged samples was investigated by measuring gas permeability before, during and after reconsolidation and water resaturation. Figure 2.3 illustrates schematically the assembly of the samples and the testing system

developed by GRS. The equipment allows simultaneous testing of four samples to determine permeability to gas or to water at injection pressures up to 10 MPa and under different confining stresses up to 25 MPa. The samples were sealed with silicon in rubber jackets and installed in an oil pressure vessel. Each sample was connected via sintered porous discs to in- / outlet lines at both end faces. Nitrogen gas or synthetic formation water was injected at the inlet. Water injection can be done either by applying gas pressure on the water surface in a gas/water vessel or using a liquid pump. For the measurements of gas permeability dry nitrogen gas was wetted through a water bath before injected into the samples in order to avoid artificial drying since the air in pores or fractures of backfill or EDZ is assumed to be saturated with water vapour. The outflow was measured at the outlet by means of partially water-filled burettes. The error in the data from the pressure transducers used for controlling the gas or water injection pressure is lower than 0.1% and the accuracy of the volumetric measurements with the burettes is ±0.05 cm^3. To avoid a possible leakage along the interface between jacket and sample, the injection pressure was checked to be lower than the external confining stress.

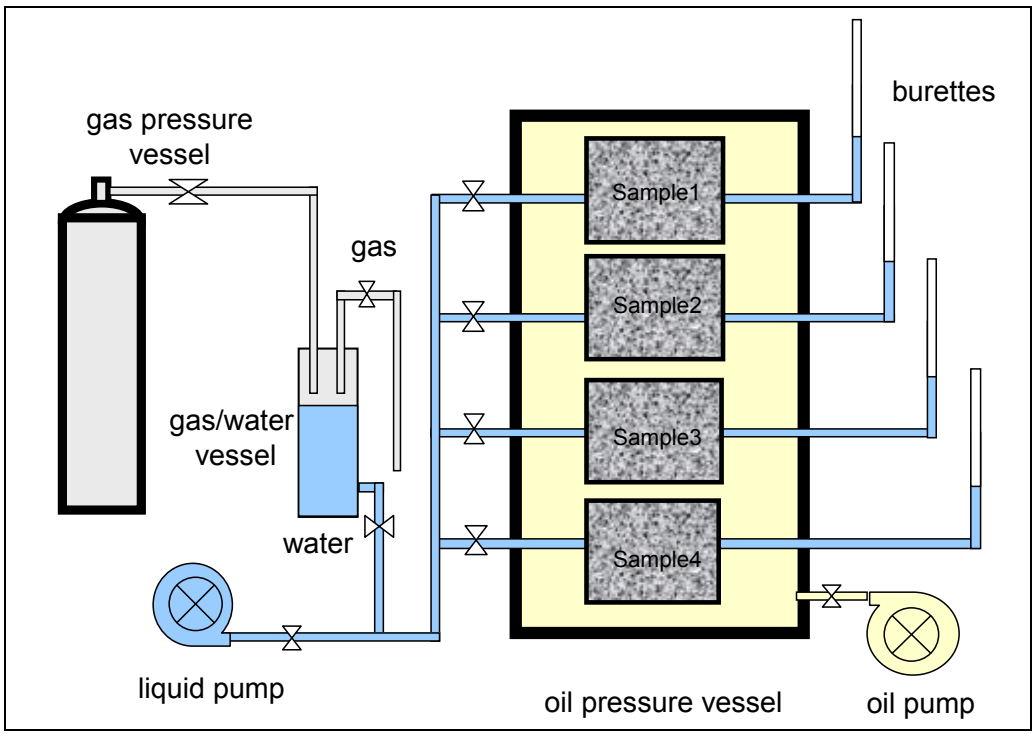

Figure 2.3 Set-up of the sealing test with damaged clay samples

2.1.3 Test procedure

The test procedure comprised of several steps:

1. **Measurement of the initial gas permeability**: In order to characterise the initial hydraulic properties of the damaged samples, gas permeability was measured as a function of time by injecting nitrogen gas at an ambient temperature of 20°C. Taking into account that the stress in the EDZ around underground openings is reduced due to rock yielding, the damaged samples were re-loaded to a low confining stress of 1.5 MPa. The injected nitrogen gas was wetted to mimic the in-situ gas conditions in the EDZ. At the outlet a relative humidity of about 40% was recorded. Because of the already existing fractures and the de-saturated pore space in the damaged samples, only a low injection pressure of 0.075 MPa was applied at the inlet. Gas outflow was measured at atmospheric pressure. The permeability measurements were performed over a period of 2.3 months.

2. **Water resaturation**: Following the gas injection phase, synthetic water made by mixing clay powder and distilled water was injected into the damaged samples under confining stresses of 1.6 to 2.0 MPa in order to simulate the water transport from the surrounding rock into the EDZ. The water injection pressure was adjusted between 0.6 and 1.0 MPa. To reach a full saturation, this water injection phase lasted for a period of 5.4 months.

3. **Reconsolidation**: Reconsolidation of the EDZ under the combined impact of rock stress and backfill pressure was simulated by applying confining stresses of 2.0 to 2.6 MPa for 4 months to the damaged samples. Obviously, the applied stresses are much lower than the lithostatic stress which will develop again in the EDZ over a period of thousands of years after closing the repository. Also, the reconsolidation phase emulated in the laboratory is clearly much shorter than in-situ. However, it was long enough to observe its effect on the sealing.

4. **Examination of sealing**: Finally, the combined effects of reconsolidation and water resaturation on the self-sealing of the damaged samples were examined by measuring the gas permeability again and comparing the results with the data obtained before. The measurement of gas permeability was also carried out at a low confining stress of 2.4 MPa and at a relatively high injection pressure of 2.0 MPa for 2.4 months.

The gas permeability was determined using Darcy's law for steady state flow of compressible fluids:

$$k_g = \frac{2 \cdot q_g \cdot \mu_g \cdot L \cdot p_o}{A \cdot \left(p_1^2 - p_o^2\right)} \qquad (2\text{-}1)$$

where k_g is the intrinsic permeability (m^2), q_g is the flow rate of the gas (m^3/s), μ_g is the dynamic viscosity of the gas (Pa·s), L is the length of the sample (m), A is the cross-section of the sample (m^2), p_o is the atmospheric pressure (Pa), p_1 is the injection pressure (Pa).

The permeability to water was determined using Darcy's law for steady state flow of incompressible fluids:

$$k_w = \frac{2 \cdot q_w \cdot \mu_w \cdot L}{A \cdot \Delta p} \qquad (2\text{-}2)$$

where k_w is the water permeability (m^2), q_w is the flow rate of the water (m^3/s), μ_w is the dynamic viscosity of water (Pa·s), L is the length of the sample (m), A is the section of the sample (m^2), Δp is the pressure difference (Pa).

2.1.4 Test results

Figure 2.4 summarises the gas permeability values measured before and after resaturation and reconsolidation of the damaged samples. Before resaturation and reconsolidation, the gas permeabilities of the two damaged samples MSE00953-4/-2 decreased steadily from the high initial values of $4 \cdot 10^{-16}$ and $9 \cdot 10^{-17}$ m^2 down to $1 \cdot 10^{-16}$ and $1 \cdot 10^{-17}$ m^2, respectively, over 68 days, indicating re-sealing of the damaged samples due to the consolidation even under the low confining stress. In contrast to that, the permeability measured on the other damaged sample MSE00953-3 is comparable to that of the undamaged reference sample MSE00953-1. This suggests that the fractures created in the damaged sample were not appreciably interconnected and did therefore not form significant continuous hydraulic pathways in the direction of injecting. The gas permeabilities of these samples decreased in the first days from $3 \cdot 10^{-20}$ m^2 down to $2 \cdot 10^{-21}$ m^2, but then gradually increased again to $3 \cdot 10^{-20}$ and $7 \cdot 10^{-20}$ m^2 over the following 20 days, and finally remained more or less constant. The

increase of the gas flow through the samples might be due to an enlargement of the effective flow pathways by flowing relatively dry gas even if it had been wetted before.

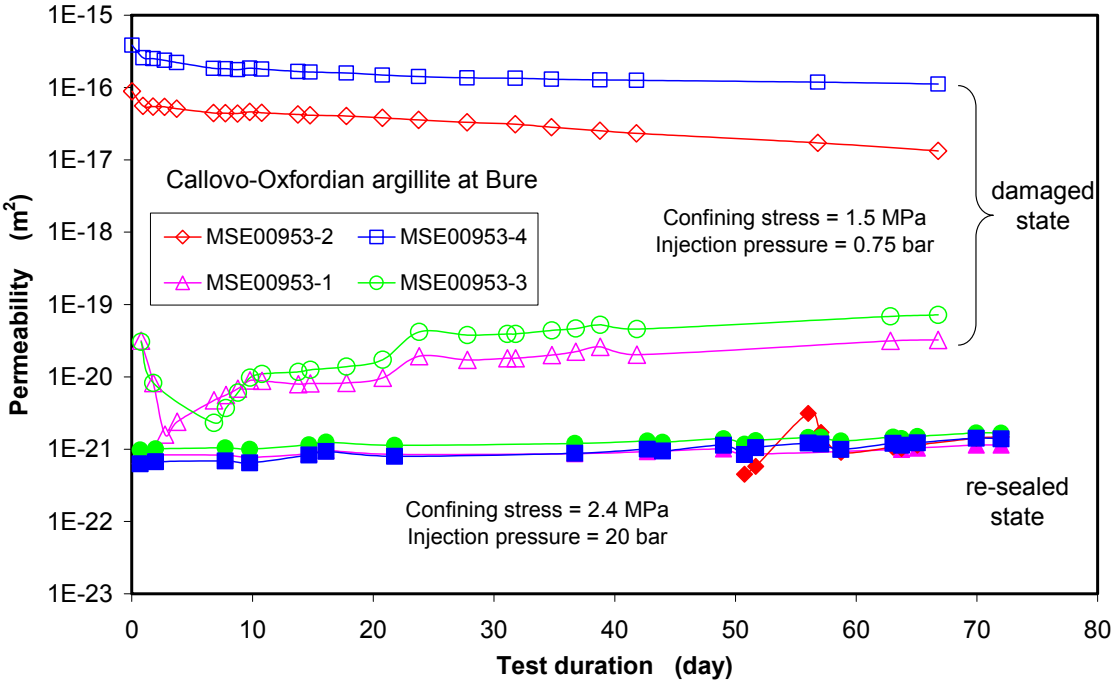

Figure 2.4 Comparison of the gas permeability of the damaged clay samples before and after resaturation and reconsolidation

In the following stage of the test procedure the samples were injected with synthetic water at pressures of 0.6 to 1.0 MPa and under confining stresses of 1.6 to 2.0 MPa over 5.4 months. The total amount of water injected into all the samples was determined to be about 80 cm^3, corresponding to an inflow rate of ~ $3.4 \cdot 10^{-4}$ cm^3/min. But no water outflow was observed at the opposite side of each sample. After testing, the water content of the samples was determined after drying at 105°C. The data are given in Table 2.

Assuming that the density and the porosity of the samples were unchanged after testing, the degree of water saturation was established for each sample.

$$S = \frac{\rho_d w}{\rho_w \phi} 100 \qquad (2\text{-}3)$$

where S is the degree of water saturation (%), w is the water content (%), ρ_w is the density of the pore water (g/cm^3), ρ_d is the dry density of the sample (g/cm^3), ϕ is the porosity (%).

Except for the not artificially damaged sample MSE00953-1, the calculated degrees of water saturation for the other samples are higher than 100%, indicating full water saturation of the samples and a slight underestimation of the porosity values.

Table 2 Examination of water saturation of the re-sealed samples after testing

Sample	Water content w (%)	Bulk density (g/cm^3)	Dry density (g/cm^3)	Porosity (%)	Degree of saturation (%)
MSE00953-1	3.95	2.46	2.37	0.12	76
MSE00953-2	7.26	2.44	2.27	0.16	104
MSE00953-3	6.92	2.46	2.30	0.15	106
MSE00953-4	7.20	2.44	2.27	0.16	103

Furthermore, one can roughly estimate the water permeability by assuming (a) a steady water flow with an averaged rate of $q_w = 3.4 \cdot 10^{-4} / 4 = 8.5 \cdot 10^{-5}$ cm^3/min for each sample, (b) the maximum sample length of L = 86 mm and the diameter of D = 86.5 mm, (c) the lower pressure difference of Δp = 0.6 MPa, and the water viscosity $\mu_w = 1.2 \cdot 10^{-3}$ Pa·s. The estimated water permeability is lower than $4 \cdot 10^{-20}$ m^2 and thus in the same order of magnitude as that of the undisturbed rock.

After the subsequent reconsolidation phase of 4 months at confining stresses of 2.0 to 2.6 MPa, gas was injected again at a confining stress of 2.4 MPa and at an injection pressure of 2.0 MPa for 2.4 months. During this period, only very low permeability values in the range of $5 \cdot 10^{-22}$ to $2 \cdot 10^{-21}$ m^2 were recorded on all the samples. These permeability values are about five orders of magnitude lower than the values measured before water resaturation and reconsolidation, and also reflect the permeability of the undisturbed rock.

After the long term sealing tests, the samples were dismantled, as shown in Figure 2.5. Comparing the photos of the samples before (Fig. 2.2) and after the testing (Fig. 2.5),

one can still clearly recognise some remaining fractures previously generated by the mechanical loading. This would imply that the damaged clay samples did not yet fully re-heal under the applied reconsolidating and rehydrating conditions. However, the pronounced reduction of the gas permeability after resaturation and reconsolidation clearly indicates that the flow pathways within the samples were re-sealed under the test conditions, providing a strong evidence for a high self-sealing capability of the clay rock.

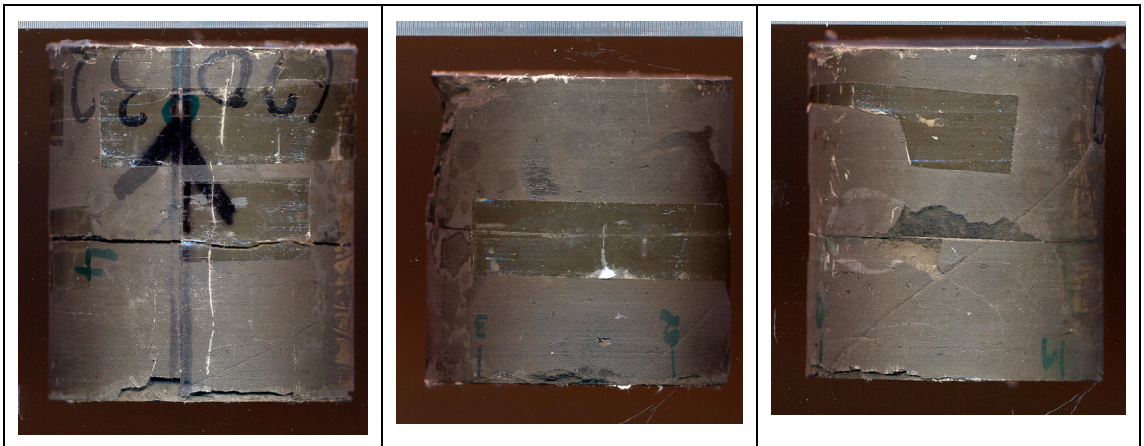

MSE00953-2 | MSE00953-3 | MSE00953-4

Figure 2.5 Photos of the strongly-damaged samples after the long-term sealing test

2.2 Tests on a hollow cylindrical sample

2.2.1 Sample preparation

In order to simulate the EDZ around a borehole, a hollow cylindrical sample (EST17284) from the Callovo-Oxfordian argillite was prepared with an outer diameter of 79 mm, an inner diameter of 20 mm, and a length of 103 mm, as shown in Figure 2.6. The sample was drilled from the vertical borehole in the axis of the main access shaft of the MHM-URL. The sampling depth was 472 m. The axis of the sample was perpendicular to the bedding plane. The sample was altered up to a certain degree due to drilling, transport, storage and preparation. The additional drilling of the central borehole in this sample is a similar process to the excavation of drifts and boreholes, leading to a certain amount of micro-fractures near the borehole wall. But no macro-cracks were visually found. A sample bulk density of 2.36 g/cm^3 and a water content of 4.3% were measured. The derived dry density is 2.27 g/cm^3 and the porosity is 16%. The degree of water saturation was calculated to be 57%.

Figure 2.6 Photos of the hollow cylindrical sample

2.2.2 Test method

The sealing tests on the hollow cylindrical sample were conducted in a triaxial apparatus (Karman type), which allows to apply a maximum axial force of 1600 kN, a maximum lateral stress of 70 MPa, a maximum temperature of 200°C, and a gas or water injection pressure up to 15 MPa. The assembly of the sample in the triaxial cell for the radial and the axial fluid injection, respectively, are shown in Figure 2.7. Outflow is measured at the outlet side by means of burettes with an accuracy of ±0.05 cm^3.

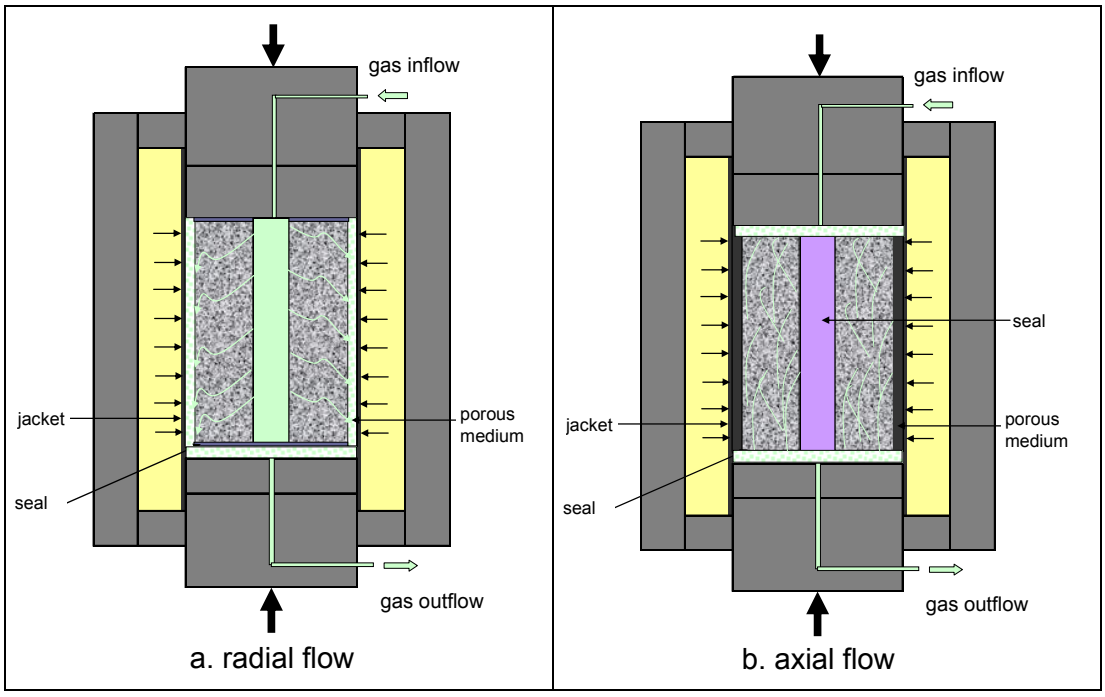

Figure 2.7 Two tests of sealing in the EDZ around a borehole

2.2.3 Test procedure

The test procedure included different phases:

- measurement of the gas permeability in both radial and axial directions as a function of external confining stress,
- re-saturation of the damaged sample by water injection, and
- determination of gas entry / breakthrough pressure and permeability of the sample after reaching a certain sealing degree.

Figure 2.8 illustrates the conditions during the test with respect to confining stress and gas / water injection.

1. **Measurement of radial gas permeability**: The hollow sample with an outer diameter of 79 mm was inserted into a rubber jacket of 100 mm diameter. The central borehole was empty and linked directly to the inlet line. At the top of the sample the interface of the sample to the upper piston was sealed with silicon to avoid flow leakage at the inlet. The bottom of the sample including the central borehole was also hydraulically separated with silicon from the sinter plate. The annulus between sample and jacket was filled with fine-grained sand, providing a hydraulic connection of the outer sample surface and the outlet line via the porous disc at the bottom.

   Confining stress was applied stepwise in 2 loading / unloading cycles. It was increased from 0 up to 15 MPa and then down to 4 MPa again in the first cycle and then from 4 MPa up to 28 MPa and finally down to 2 MPa in the second cycle. Because of the cylindrical inner opening, the axial stress acting on the ring-like cross section of the sample was slightly higher than the radial stress. But the stress distribution in the hollow sample was inhomogeneous and time-dependant since radial stress at the inner borehole wall was equal to the gas pressure. The highly concentrated deviatoric stress state in the area near the inner borehole might have generated micro- and macro-fractures. Unfortunately, the creation and development of the EDZ around the borehole could not be monitored because of difficulties with the instrumentation in such a small borehole.

   Under different confining stresses, nitrogen gas was injected into the borehole at a constant pressure of 0.17 MPa and gas flow through the sample in radial direction was measured over 2 months (cf. Fig. 2.7a). From these measurements, the values of gas permeability in radial direction can be determined as a function of the

confining stress. Each measuring interval lasted over of several days. After reaching a steady-state gas flow, Darcy's law for compressive media could be used for the calculation of radial gas permeability of the hollow sample:

$$k_g = \frac{q_g \cdot \mu_g \cdot p_0}{\pi \cdot L \cdot \left(p_1^2 - p_0^2\right)} \ln \frac{r_1}{r_2} \qquad (2\text{-}4)$$

where r_1 is the inner radius (m) and r_2 is the outer radius (m). The meanings of the other symbols are given in equation (2-1).

2. **Measurement of axial gas permeability**: After the first test phase, the sample was removed from the cell. The seals at the top and the bottom of the sample were detached and instead, the borehole as well as the annular space between the sample and jacket was carefully sealed with silicon. Subsequently, the sample was placed between two porous discs at the top and the bottom, put back into the cell, and reloaded up to a maximum external stress of 26 MPa. Because of the sealing of the borehole and the incompressibility of the filling material, the external compression could result in a pressure build-up at the borehole wall and hence the hollow sample was probably compacted. In order to create more damage, deviatoric stresses were then applied to the sample by changing the radial stress and the axial stress. Under different deviatoric stresses, nitrogen gas was injected at the top of the sample by the same injection pressure of 0.17 MPa as in the first phase. The gas flow through the sample in axial direction was measured at the bottom outlet (cf. Fig. 2.7b). Based on the measurement of the axial gas flow, the axial gas permeability can be calculated according to Darcy's law in the form of (2-1). This test phase lasted over 2.3 months.

3. **Water resaturation**: Water transport from the surrounding rock to the EDZ around a borehole was simulated in the laboratory test by injecting synthetic pore water to the sample. At a confining stress of about 2 MPa, a constant water pressure of 1.0 MPa was imposed to the bottom of the sample over 1.7 months.

4. **Gas breakthrough test**: After the resaturation of the stressed sample, a re-sealing up to a certain degree could be achieved due to the long term reconsolidation and rehydration. To determine the degree of re-sealing of the damaged sample, nitrogen gas was injected again at the top of the sample, i.e. the opposite side of the previous water injection. At confining stresses of 2 to 2.8 MPa, the gas

injection pressure was increased step by step to detect gas breakthrough pressure. After gas breakthrough, the gas pressure was reduced to a lower level of 0.5 MPa to measure the gas permeability as a function of time.

2.2.4 Test results

Characteristic test conditions during all four test phases described above are plotted in Figure 2.8. The applied axial and radial stresses as well as the gas and water injection pressures are given.

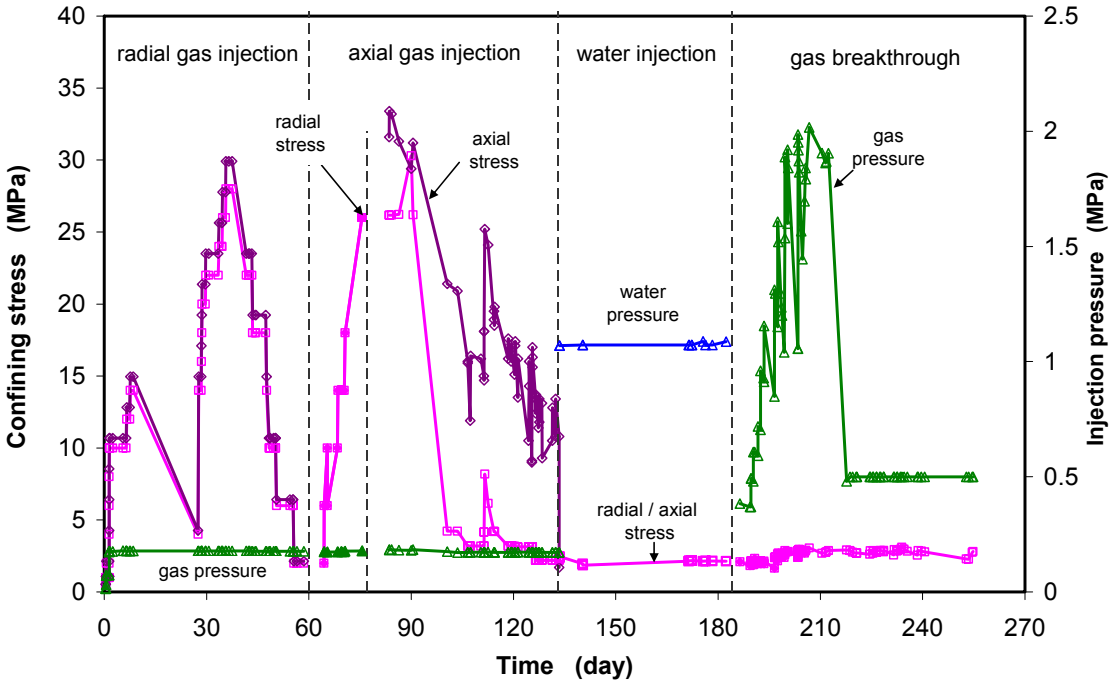

Figure 2.8 Course of the test with a hollow clay sample represented by the confining stress and fluid pressure

2.2.4.1 Radial gas permeability

Figure 2.9 shows the radial gas permeabilities measured during phase 1 as a function of the confining stress on the hollow clay sample. The initial permeability values at a confining stress of 1 MPa were in the order of 10^{-15} m^2. Increasing the confining stress to 28 MPa led to a significant reduction of the permeability down to $5 \cdot 10^{-21}$ m^2, being about 6 orders of magnitude lower than the initial values. At stresses above 30 MPa, no outflow of gas was detected. In fact, the tangential and axial stress components in

the cylinder are increased by the application of external confining stress leading to the compression of the pre-existing cracks, which were mainly distributed along the horizontal bedding planes. Additionally, the radial gas permeability was also measured along the unloading path. The k-values obtained at the decreased stresses from 26 to 4 MPa are about two orders of magnitude lower than those obtained along the previous loading path. This indicates a pronounced plastic closure of the fractures by the previously applied stress. The dependence of the permeability on the confining stress can be reasonably well expressed by an exponent equation.

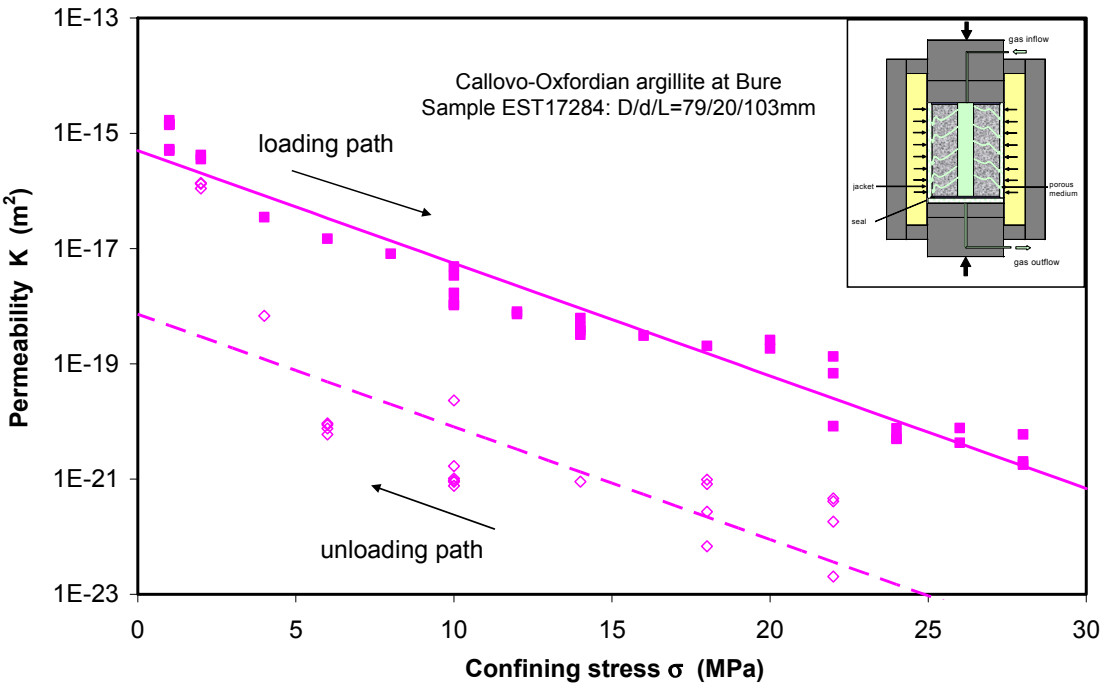

Figure 2.9 Radial gas permeability of the hollow clay sample as a function of confining stress

2.2.4.2 Axial gas permeability

Figure 2.10 shows the axial gas permeabilities as a function of the confining stress on the sample with the sealed borehole. Increasing the external stress resulted in an exponential reduction of the axial gas permeability. In fact, the application of external stress on the sealed hollow sample produced a back-pressure in the sealing material. Under the impact of the external stress and inner back-pressure, the pre-existing flow pathways along the sample length were compressed and even closed by the normal (radial) stress.

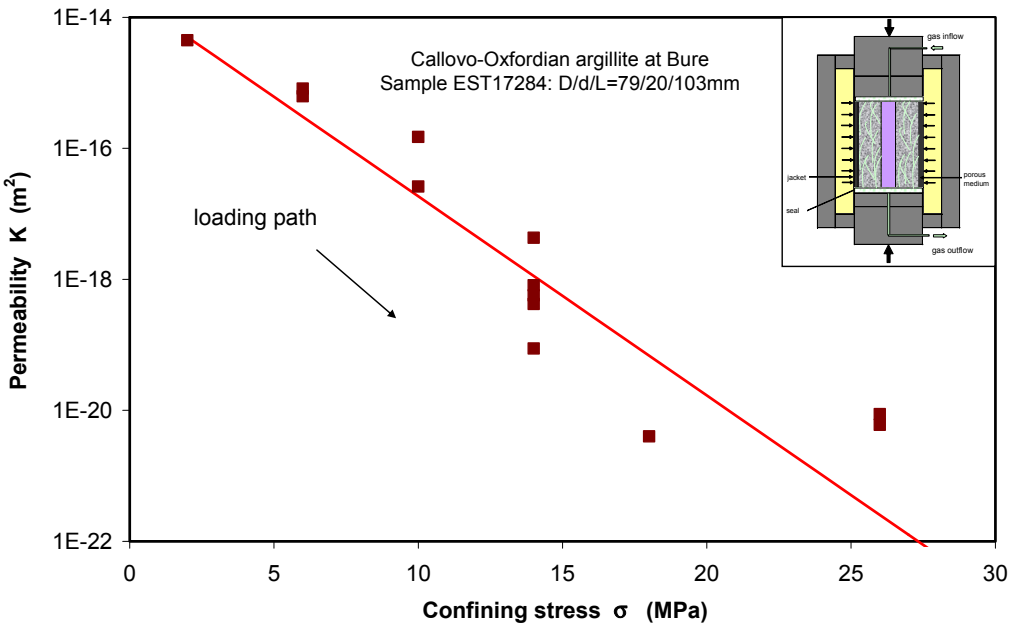

Figure 2.10 Axial gas permeability of the hollow clay sample as a function of confining stress

Figure 2.11 compares the axial and radial gas permeability of the sample. It is obvious that at confining stresses lower than ~14 MPa, the axial permeability is up to 1 order of magnitude higher than the radial one determined along the loading path. The hydraulic anisotropy vanishes with increasing the confining stress.

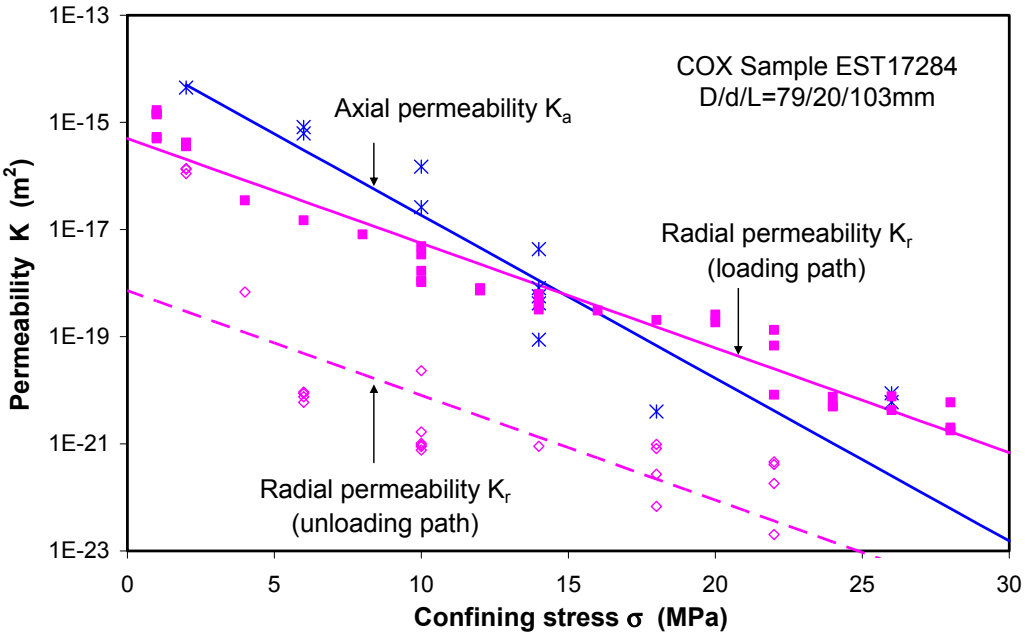

Figure 2.11 Axial and radial gas permeability of the hollow clay sample

Additionally, the sample was further damaged by increasing axial stress at constant lateral stress, whereby the axial gas permeability was measured (cf. Fig. 2.8). The k-values obtained are depicted in Figure 2.12 as function of the mean stress ($\sigma_m = (\sigma_a + 2\sigma_r) / 3$). It can be seen that the permeability decreases with increasing mean stress. The dependency of the permeability on the deviatoric stress ($\Delta\sigma = \sigma_a - \sigma_r$) is illustrated in Figure 2.13. Although the data show a relatively large scatter, one can still recognise that the permeability tends to decrease with increasing the deviatoric stress in the test range. Note, that the stress state mentioned above is not representative for the local state in the cylindrical sample due to the different filling material in the borehole.

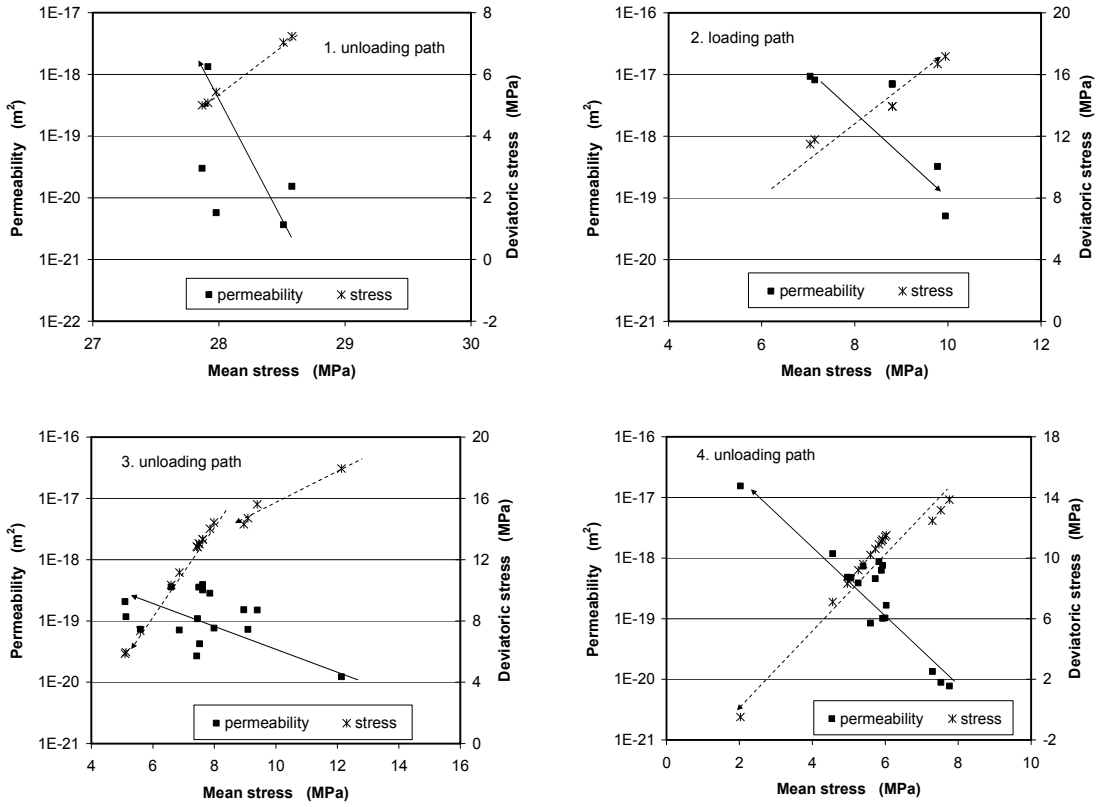

Figure 2.12 Axial gas permeability measured during deviatoric loading at constant lateral stress

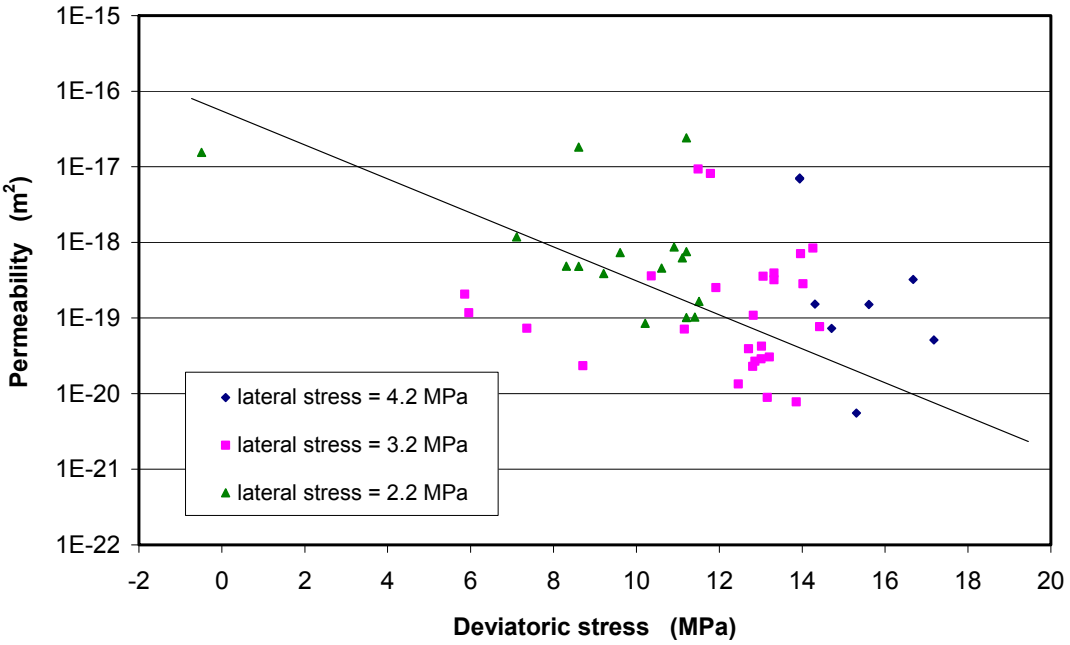

Figure 2.13 Axial gas permeability as a function of the deviatoric stress

2.2.4.3 Water resaturation

After measuring radial and axial gas permeability, the sample was injected with synthetic pore water at the bottom at a pressure of 1 MPa under a confining stress of 2 MPa. The water inflow rate and the accumulated water uptake are shown in Figure 2.14. The initial inflow rate was recorded to be $2 \cdot 10^{-3}$ cm^3/min which decreased steadily with time down to $2 \cdot 10^{-4}$ cm^3/min after 50 days. About 20 cm^3 of water had been injected at the end of the resaturation phase, which is about 4.3% of the sample volume and corresponds to an increase of the water content of 7.1%. By adding this value to the initial value of 4.3%, the total water content at the end of this test phase amounts to approximately 11.4%. Assuming the initial porosity remained unchanged, an actual degree of water saturation after the water injection of 123% was calculated, indicating a fully-re-saturated state and a pore volume increase. Although no water outflow was detected, the water permeability can roughly be estimated and a maximum of $7 \cdot 10^{-20}$ m^2 was calculated, which lies in the same order of magnitude as that of the undisturbed rock.

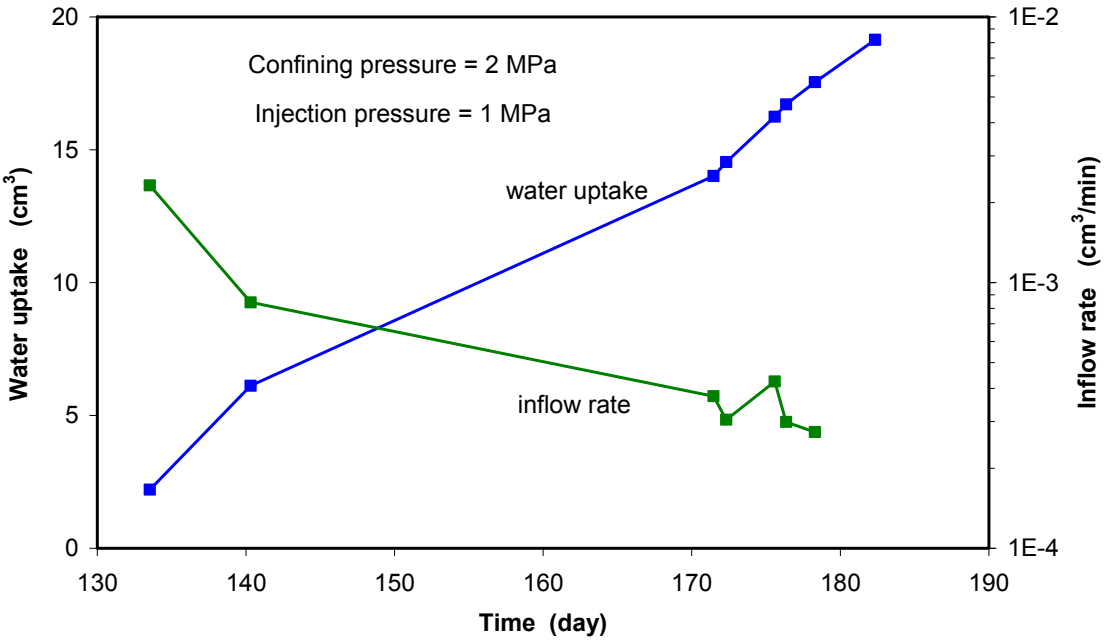

Figure 2.14 Water inflow rate and accumulated water uptake

2.2.4.4 Gas breakthrough pressure

After water resaturation, nitrogen gas was injected again at the top of the sample opposite to the location of water injection in the previous test phase. The aim of this test phase was to determine the gas breakthrough pressure of the re-sealed sample and to measure the gas permeability after breakthrough. Figure 2.15 shows the applied confining stresses and gas injection pressures as well as the resulting axial gas permeability. Under the confining stresses of 1.9 to 2.3 MPa and gas pressures of 0.8 to 1.8 MPa, no gas outflow was observed within the first 20 days. After that, a very low gas permeability round $5 \cdot 10^{-22}$ m^2 could be recorded, and then a gas breakthrough followed at a gas pressure of about 1 MPa and a confining stress of about 2.8 MPa. At gas breakthrough, the gas outflow rate increased rapidly according to the high permeability of $7 \cdot 10^{-16}$ m^2, which was then six orders of magnitude higher than before. After breakthrough, however, the gas permeability dropped to 10^{-18} m^2 and remained at that value. This observation suggests that some of the re-sealed fractures were reopened by the gas pressure and then closed again under compressive stress conditions.

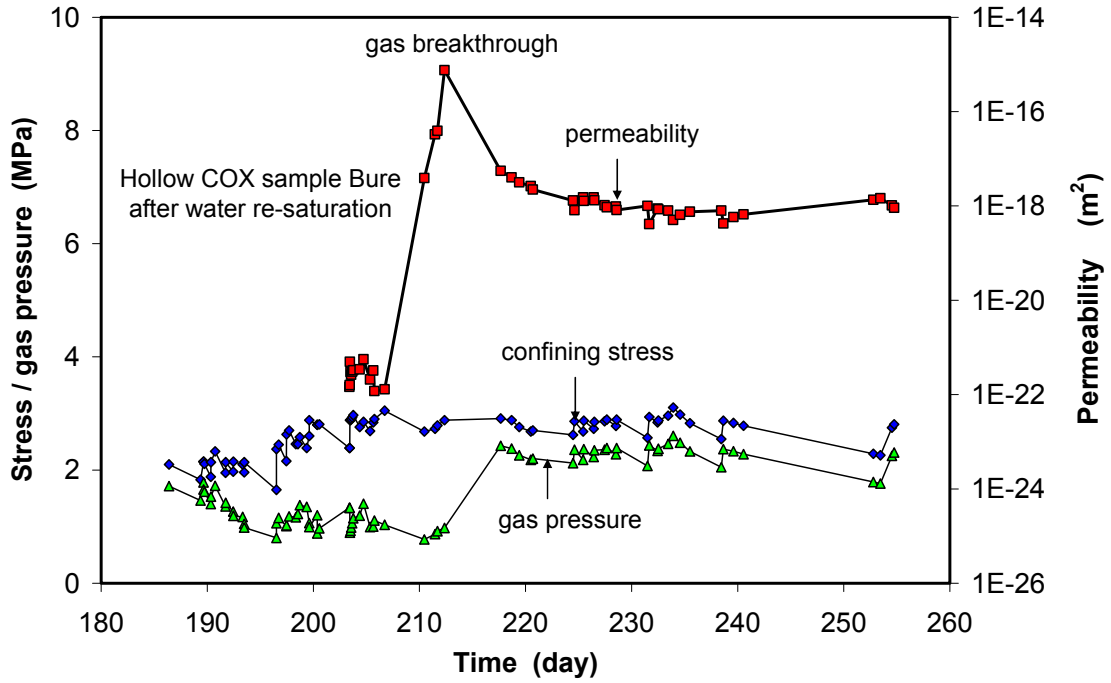

Figure 2.15 Gas breakthrough pressure and permeability of the re-sealed clay sample

The sealing test was terminated after 8.5 months. Subsequently, the sample was dismantled, as shown in Figure 2.16. One can clearly recognise that the sample was strongly damaged showing large and interconnected fractures inclined to the axis at angels between 0° and 35°. Under the applied test conditions, however, the fractures were more closed, indicated by the observations of the high gas breakthrough pressure and the very low permeabilities to gas and to water.

Figure 2.16 Dismantled sample after the test

2.3 Tests on a large sample

Originally, GRS proposed to conduct large-scale sealing tests on big hollow cylindrical samples. However, because of the mechanical instability of the layered cores, it was not possible to drill and prepare usable samples of the envisaged dimensions, and thus the proposed tests could not be carried out despite best effort. The test program was therefore slightly modified using a large Opalinus clay sample without a central borehole.

2.3.1 Sample preparation

Several large Opalinus clay cores of 260 mm diameter and lengths between 1.0 to 2.5 m were drilled from the HE-D heater borehole in the Mont-Terri-URL /ZHA 07a/. Visual inspection let them appear to be very compact and relatively homogeneous. Immediately after coring, the cores were sealed air-tightly in aluminium foils, covered by rubber jackets, and confined by pressing plastic tubes over the jackets using stretching bands. After a storage period of more than 1 year, the cores were unpacked for the heating tests. However, some fissures appeared on the surfaces which were more or less aligned with the bedding planes. One sample from the area near the drift wall showed macro-fractures extending axially through the sample. During the following year, more fractures appeared, as shown in Figure 2.17. This “naturally” fractured sample may represent a realistic state of the in-situ EDZ and thus provides an optimal initial condition for laboratory tests on its self-sealing behaviour. This sample was carefully prepared by cutting and planishing the end faces to a size of 616 mm length and 260 mm diameter. The following petrophysical properties of the sample were measured: a grain density of 2.71 g/cm^3, a bulk density of 2.41 g/cm^3, a dry density of 2.27 g/cm^3, a porosity of 16.5%, a water content of 6.3%, and a degree of water saturation of 86%.

2.3.2 Test method

The large-scale sealing test was performed in the MTS big triaxial apparatus at GRS’ laboratory, which allows THM tests with a maximum load of 50 MPa lateral stress and 75 MPa axial stress, a maximum temperature of 150°C and a maximum fluid pressure of 15 MPa.

top bottom

Figure 2.17 Preparation of a large Opalinus clay sample with macro-cracks

Figure 2.28 shows the test apparatus, the test assembly, and the sample installation. The large sample was inserted in a jacket and covered by porous discs at the top and at the bottom. The axial and radial loads were controlled individually by servo-regulation of the oil pressures in the axial load cylinder and in the triaxial cell with an error of less than 0.1%. The axial strain was measured by a LVDT deformation transducer mounted in the lower piston outside the cell with an error of less than 0.1%. The measurement of the radial strain was performed by using a MTS circumferential extensometer installed outside the jacket around the sample with an error of less than 0.2%. The permeability measurement was conducted by injecting the sample with nitrogen gas at the bottom at a constant pressure and by monitoring gas outflow at the top using a graduated burette.

MTS triaxial testing system

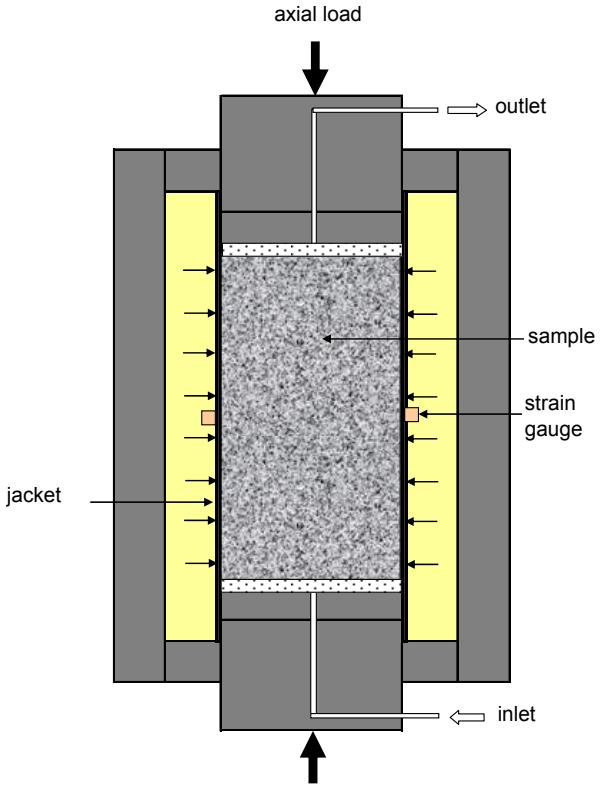

test assembly

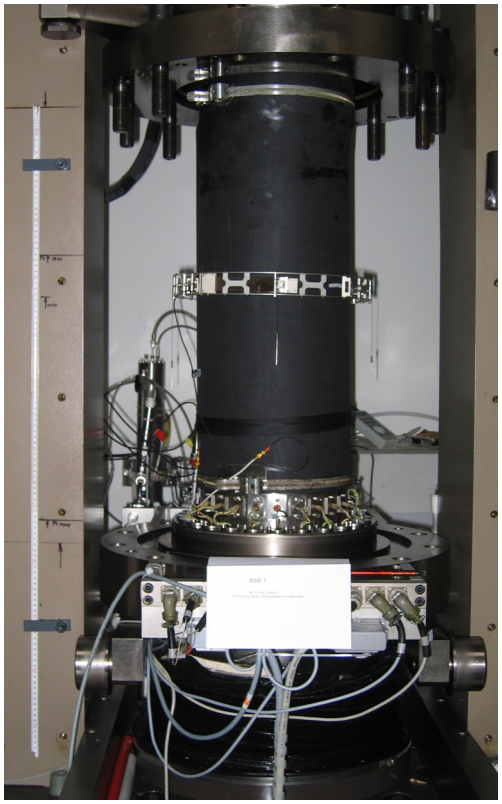

sample installation

Figure 2.18 Large-scale sealing test on an Opalinus clay sample in the MTS triaxial apparatus at GRS' laboratory

2.3.3 Test procedure

Similar to the previously mentioned tests, the large-scale sealing test was conducted in several steps to

1. examine the impact of normal (radial) stress on gas permeability along the fractures oriented parallel to the sample axis,
2. resaturate the damaged sample by injection of synthetic formation water, and
3. determine the gas permeability of the sample after a long-term reconsolidation and resaturation phase of more than 4 months.

The whole test procedure is illustrated in Figure 2.19 showing the applied confining stresses and the measured permeability.

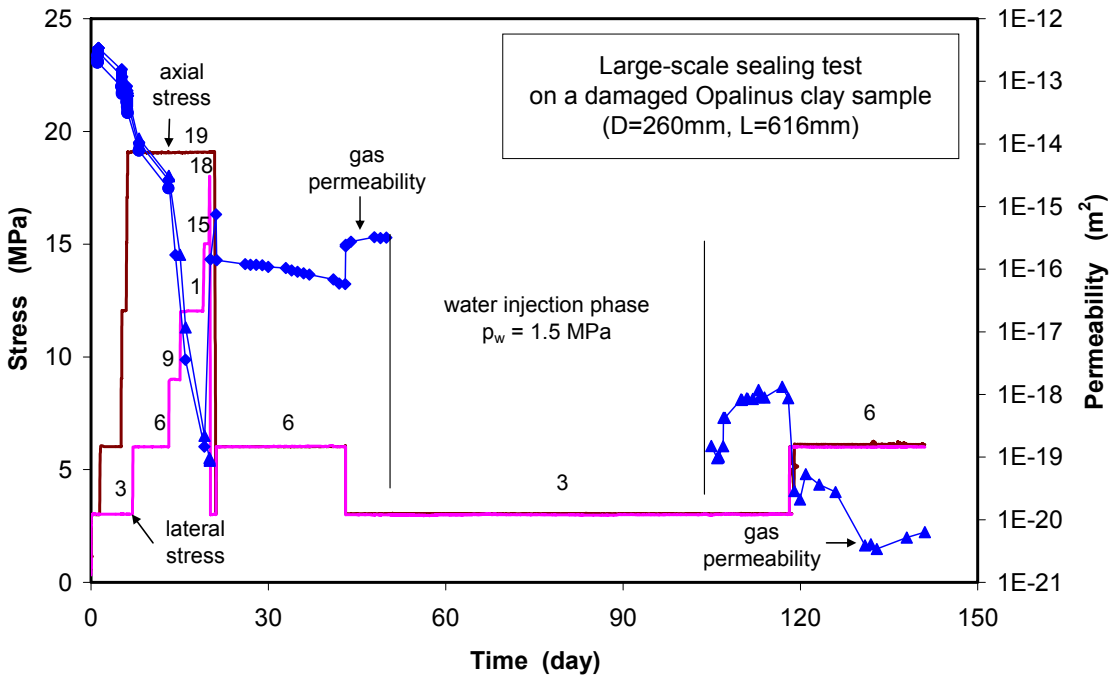

Figure 2.19 Procedure of the large-scale sealing test on a fractured Opalinus clay sample in terms of the applied confining stress and the measured permeability

2.3.4 Test results

The main observations from the large-scale sealing test are summarised as follows:

- At an isotropic stress of 3 MPa, an initial gas permeability of 10^{-13} m^2 for the strongly-fractured sample was determined. This value represents the in-situ permeability of 10^{-13} to 10^{-15} m^2 well that was observed near the drift wall in the Mont-Terri-URL. In order to examine the impact of the major principle stress on permeability in the fracture direction, the axial stress was increased from 3 to 19 MPa. Generally, the increase of the axial stress should generate an extension of the fractures in radial direction and thus a high permeability through the enlarged fractures. But an unexpected permeability reduction down to 10^{-14} m^2 was observed. This might be interpreted as the collapse of some fractures and thus decrease of the flow pathways.

- The impact of normal stress on the permeability of the fractured sample was investigated by increasing the radial stress from 3 to 18 MPa. Figure 2.20 shows the measured permeability data as a function of radial stress. The increase of stress applied in the test led to a dramatic decrease of permeability from $7 \cdot 10^{-14}$ m^2 down to $1 \cdot 10^{-19}$ m^2, which is about five orders of magnitude lower than the initial value. This suggests a strong impact of normal stress on the closure of fractures. After unloading to 6 MPa, a progressive reduction of the gas permeability was observed from $1 \cdot 10^{-16}$ m^2 down to $5 \cdot 10^{-17}$ m^2 over 22 days (Fig. 2.19). As the radial stress was decreased to the initial level of 3 MPa, the permeability increased to $2 \cdot 10^{-16}$ m^2, which is still more than two orders of magnitude lower than the initial value of $7 \cdot 10^{-14}$ m^2 at the same stress. The significant irreversibility of the permeability changes indicates a plastic closure of the fractures to a high degree.

- The subsequent water injection was performed at a pressure of 1.5 MPa over 53 days, during which no water outflow was observed at the opposite side. After that, gas was injected again at a pressure of 0.5 MPa and a low permeability of $1 \cdot 10^{-19}$ m^2 was recorded. Increasing the gas pressure to 0.7 MPa accelerated the gas flow concurrent with an increase of permeability to $1 \cdot 10^{-18}$ m^2 (cf. Fig 2.21). These permeability values are 2 to 3 orders of magnitude lower than those observed before water injection, namely $1 \cdot 10^{-16}$ m^2. It has to be pointed out that because of the large sample size and the relatively short water injection time, the fractures in the sample might be only partly resaturated and re-sealed. Therefore, the fractures might be easily reopened by relatively low injection pressures. An

additional stress increase from 3 to 6 MPa reduced the permeability to significantly less than 10^{-20} m^2, which is about the permeability of the intact rock. After the test, many of the pre-existing cracks on the surfaces vanished.

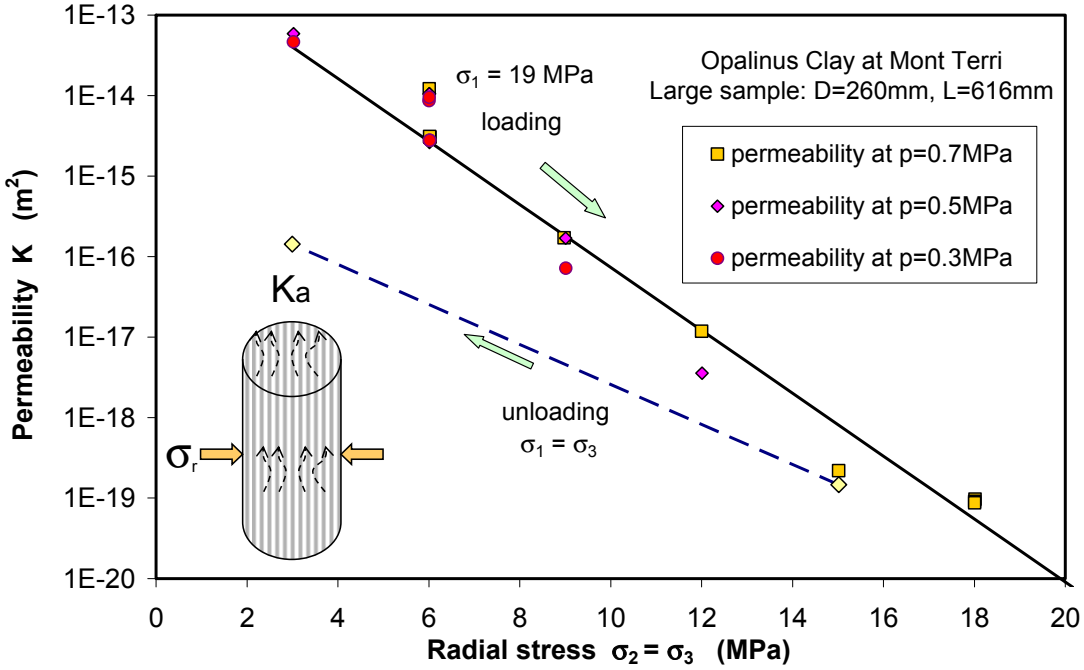

Figure 2.20 Gas permeability of the fractured sample as a function of the normal stress along loading and unloading paths

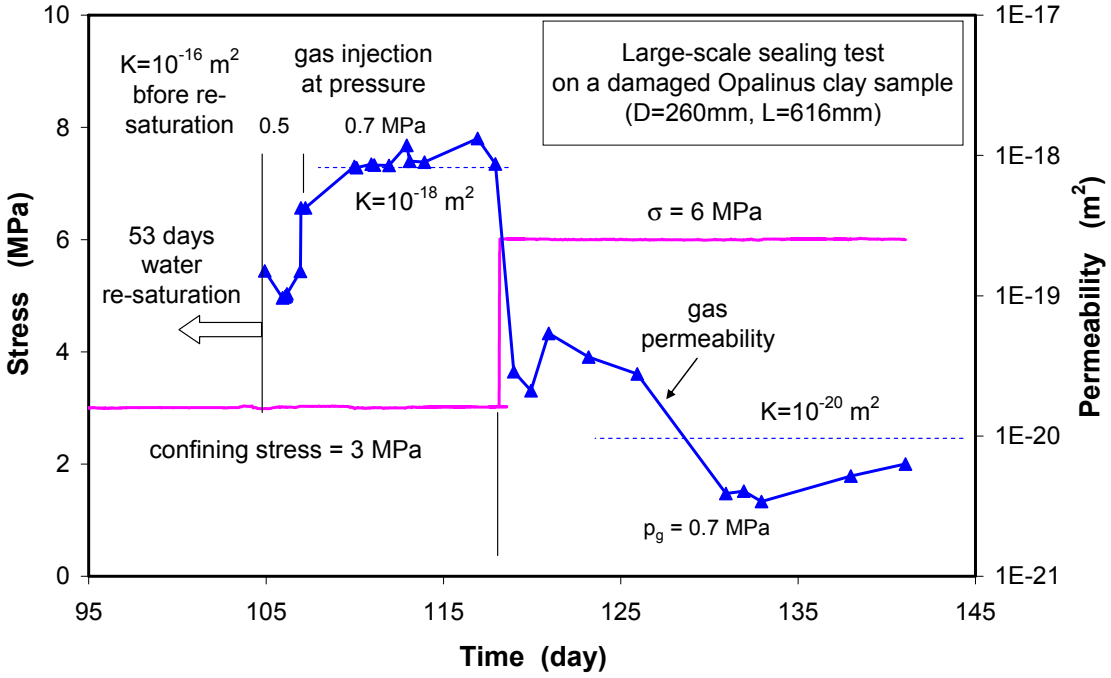

Figure 2.21 Comparison of the gas permeability of the fractured sample before and after water resaturation

The large-scale fractured sample is representative for the rock mass in the EDZ and the test conditions are equivalent to those in a repository at depths between 400 m to 600 m. The results of the laboratory sealing tests may therefore be transferable to an in-situ real repository site, but the sealing process observed in the laboratory in months and years is much shorter than that in-situ in hundreds or thousands of years. The prediction of the long-term sealing process in-situ needs physically-based constitutive models which have to be developed on basis of the short-term laboratory experiments.

3 Modelling work

Recently, a number of constitutive models has been developed for the description of the thermo-hydro-mechanical behaviour of clay rocks /VAU 03/04/, /GRG 06/, /JIA 06/, /HOX 06/, /SU 07/, /GEN 07/. For the short-term mechanical behaviour, various elasto-plastic models are available with or without softening / hardening, damage evolution and THM coupling. The time-dependent deformation is described by visco-plastic models with or without damage. Most of the models have been implemented in various numerical codes and applied for the analysis of deformation and damage of the Callovo-Oxfordian argillite during the shaft sinking at the MHM-URL /SU 07/. Significant advances in the capability of the models to reproduce the in-situ observed phenomena were obtained. However, it was recognised that further improvements of the models are necessary to forecast the hydro-mechanical coupling and the long-term evolution and self-sealing of the EDZ.

In the framework of this project, GRS originally planned to model laboratory damage-sealing tests on large hollow clay samples for validating the suitability of a clay damage model developed by Vaunat et al. /VAU 03/04/. This model has been implemented in CODE-BRIGHT /UPC 04/. Because the proposed large-scale tests could not be conducted as mentioned in section 2.3, the envisaged modelling was impossible. But for the design of the planned tests, pre-operational calculations were carried out und the results are reported herein.

3.1 Damage-elastoplastic model

A damage-elastoplastic model was developed by Vaunat et al. /VAU 03/04/ for indurated clays, assuming argillaceous rock to be a composite material made of a clay matrix connected by bonds (Figure 3-1). The clay matrix behaves like a typical elastoplastic soil, while the bonds behave like a typical quasi-brittle material that can be represented by a damage elastic law. The stress / strain behaviour of the composite material is determined by coupling both responses of matrix and bonds under compatible conditions. In order to gain a better understanding of the model features, this model is described in more detail below, based on the literature of /VAU 03/04/, /UPC 04/.

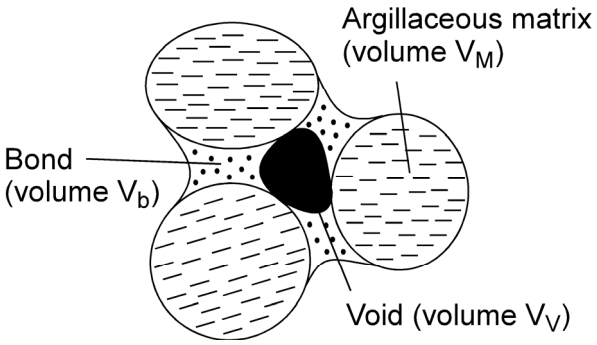

Figure 3.1 Schematic arrangements of clay matrix and bonds in argillaceous rock

3.1.1 Definitions

The solid phase has two components, each one occupying a given volume fraction of the porous medium. Clay matrix volume is noted as V_M and the bond volume as V_b. The sum is the volume of the solid phase:

$$V_S = V_M + V_b \tag{3-1}$$

Different void ratios and volumetric strains are defined:

Void ratio: $$e = V_V / V_S \tag{3-2}$$

Pore volumetric strain: $$\varepsilon_v = -de/(1+e) \tag{3-3}$$

Bond ratio: $$e_b = V_b / V_S \tag{3-4}$$

Bond volumetric strain: $$\varepsilon_v^b = -de_b/(1+e) \tag{3-5}$$

Matrix ratio: $$e_M = (V_b + V_V)/V_S \tag{3-6}$$

Matrix volumetric strain: $$\varepsilon_v^M = -de_M/(1+e) \tag{3-7}$$

Relationships: $$e_M = e + e_b \tag{3-8}$$

$$\varepsilon_v^M = \varepsilon_v + \varepsilon_v^b \tag{3-9}$$

The matrix ratio e_M is a measure of the amount of volume not occupied by clay particles. The bonds are assumed to behave like a porous medium and are thus

(among other things) compressible (Eq. 3-5). It follows that the matrix (or external) volumetric strain ε_v^M is the sum of the pore volumetric strain ε_v and the bond volumetric strain ε_v^b. It is also extended to the shear strain by the expression:

$$\varepsilon_q^M = \varepsilon_q + \varepsilon_q^b \tag{3-10}$$

where ε_q^M is the matrix (external) shear strain, ε_q is the shear strain between the clay particles and ε_q^b is the shear strain in bonds.

In CODE-BRIGHT, model equations are written adopting the conventions commonly used in soil mechanics where p > 0 and ε_v > 0 depict compression:

Mean effective stress: $$p = \tfrac{1}{3}(\sigma'_x + \sigma'_y + \sigma'_z) \tag{3-11}$$

where $\sigma'_x, \sigma'_y, \sigma'_z$ are the effective stresses.

Deviatoric stress tensor: $$\mathbf{s} = \boldsymbol{\sigma}' - p\mathbf{I} \tag{3-12}$$

Second stress invariant: $$J = \sqrt{\tfrac{1}{2} trace(\mathbf{s} : \mathbf{s})} = \frac{1}{\sqrt{3}} q \tag{3-13}$$

$$q = \tfrac{1}{\sqrt{2}} \sqrt{(\sigma'_x - \sigma'_y)^2 + (\sigma'_y - \sigma'_z)^2 + (\sigma'_x - \sigma'_y)^2 + 6(\tau'_{xy} + \tau'_{yz} + \tau'_{zx})} \tag{3-14}$$

where q is the deviatoric stress, $\tau'_{xy}, \tau'_{yzy}, \tau'_{zx}$ are the shear stresses.

Lode's angle: $$\theta = -\tfrac{1}{3} \sin^{-1}(1.5\sqrt{3}\, \det \mathbf{s} / J^3) \tag{3-15}$$

3.1.2 Elastoplastic model for clay matrix

The clay matrix is modelled by an elastoplastic model using Hoek & Brown's criterion for the yield surface.

Elastic law: $$d\sigma_{ij}^M = D_{ijkl}^{eM} \left(d\varepsilon_{kl}^M - \delta_{kl} \frac{ds}{K_s^M} - d\varepsilon_{kl}^p \right) \tag{3-16}$$

where σ_{ij}^{M} = stresses prevailing at clay particles contact

D_{ijkl}^{eM} = mechanical elastic stiffness matrix of the clay

$d\varepsilon_{ij}^{M}$ = total strains of clay matrix (equal to the external strains)

K_{s}^{M} = bulk modulus against suction changes

$d\varepsilon_{ij}^{p}$ = plastic strains of the clay matrix.

Assuming linear elasticity, the elastic stiffness D_{ijkl}^{eM} is determined by Young's modulus E^{M} and Poisson's ratio ν^{M} of the clay matrix. Volumetric strain of the clay matrix induced by wetting or drying is linearly determined by the bulk modulus K_{s}^{M} which is considered to follow:

$$d\varepsilon_{v}^{s} = \frac{ds}{K_{s}^{M}} \tag{3-17}$$

Yield function (Hoek & Brown):

$$F^{p} = \frac{4\sin^{2}\left(\theta^{M} - \pi/6\right)}{R_{c}^{M}}\left(J^{M}\right)^{2} + \frac{2m^{M}\sin\theta^{M}}{\sqrt{3}}J^{M} - m^{M}\left(p^{M} + p_{t}^{M}\right) \geq 0 \tag{3-18}$$

where p_{t}^{M} = tensile strength of the clay matrix

R_{c}^{M} = uniaxial compressive strength of the clay matrix

m^{M} = parameter defining the shape of the yield surface (= R_{c}^{M} / p_{t}^{M}).

For triaxial compressive conditions, Lode's angle $\theta = -\pi/6$, the yield function is expressed as

$$F^{p} = \frac{\left(q^{M}\right)^{2}}{R_{c}^{M}} + \frac{m^{M}}{3}q^{M} - m^{M}\left(p^{M} + p_{t}^{M}\right) \geq 0 \tag{3-19}$$

The dependence of the strength R_{c}^{M} on suction is described by

$$R_{c}^{M}(s) = R_{c}^{M}(0)\left[\left(1 - r^{M}\right) + r^{M}\exp\left(-\beta^{M}s\right)\right] \tag{3-20}$$

where the coefficient r^{M} depicts the limit strength by $r^{M} = \lim_{s\to\infty}\left(R_{c}^{M}(s)/R_{c}^{M}(0)\right)$ and β^{M} defines the change rate of the strength R_{c}^{M} with suction *s*.

Plastic potential:

$$G^p = \frac{4\sin^2\left(\theta^M - \pi/6\right)}{R_c^M}\left(J^M\right)^2 + \frac{2m^M \sin\theta^M}{\sqrt{3}} J^M - \omega^M m^M\left(p^M + p_t^M\right) \geq 0 \qquad (3\text{-}21)$$

where ω^M is a parameter defining the non-associativity of the plastic flow: ω^M = 1 when associated and ω^M = 0 for zero dilatancy. Taking the associativity of the plasticity (ω^M = 1) for triaxial compressive conditions ($\theta = -\pi/6$) into account, the plastic potential has the same form as equation (3-19).

Hardening law:

A hardening/softening law is introduced through the following dependency of the tensile strength on the plastic strain:

$$p_t^M = \frac{R_{c0}^M}{m^M}\left[1 - \left(1-\alpha^M\right)\frac{\max\left(\varepsilon_1^{pM}, \xi_r^M\right)}{\xi_r^M}\right]^2 \qquad (3\text{-}22)$$

where R_{c0}^M = uniaxial compressive strength of the intact clay

ε_1^{pM} = major principal plastic strain

ξ_r^M = accumulated major principal plastic strain at which the residual strength $\alpha^{M2} R_{c0}^M$ is reached

α^M = brittleness parameter relating the intact and residual uniaxial compressive strength R_{c0}^M and R_{cres}^M by

$$\alpha^M = \sqrt{\left(\frac{R_{cres}^M}{R_{c0}^M}\right)^2 + \frac{2}{3} m^M \frac{R_{cres}^M}{R_{c0}^M}} \qquad (3\text{-}23)$$

α^M = 1 means perfect plasticity and α^M = 0 indicates total degradation (residual strength R_{cres}^M = 0).

Viscoplastic strain:

The time dependency of the plastic strain is considered as:

$$d\varepsilon_{vp}^M = \frac{dt}{\eta^M}\frac{\partial G_M}{\partial p_M}\left\langle F^p \right\rangle \qquad d\varepsilon_{vq}^M = \frac{dt}{\eta^M}\frac{\partial G_M}{\partial q_M}\left\langle F^p \right\rangle \qquad (3\text{-}24)$$

where $\langle\ \rangle$ = Macauley bracket

dt = time increment

η^M = viscosity of the clay matrix.

3.1.3 Damage-elastic model for bonds

Damage elasticity is considered for bonds in an argillaceous rock.

Elastic law: $$d\sigma_{ij}^{b} = D_{ijkl}^{eb}\left(d\varepsilon_{kl}^{b} - d\varepsilon_{kl}^{d}\right) \tag{3-25}$$

where σ_{ij}^{b} = stresses inside bonds

D_{ijkl}^{eb} = secant damaged elastic stiffness matrix of bonds

$d\varepsilon_{ij}^{b}$ = strains of bonds

$d\varepsilon_{ij}^{d}$ = damage strains.

The damaged elastic matrix is related to the undamaged elastic matrix tensor D_{ijkl}^{eb0} by

$$D_{ijkl}^{eb} = e^{-L} D_{ijkl}^{eb0} \tag{3-26}$$

where L is the damage variable related to the ratio of bond micro-cracks area over the whole bond area D, $L = \ln\left(1/\left(1-D\right)\right)$, D = 0 (L = 0) means no damage, while D = 1 ($L \rightarrow \infty$) indicates full damage of the bonds. The elastic matrix D_{ijkl}^{eb0} is defined by Young's modulus E^{b0} and Poisson's ratio ν^{b0} of the undamaged bonds through the linear isotropic elasticity. Therefore, the damage variable is explicitly related to the stiffness degradation by

$$L = \ln\frac{K^{b0}}{K^{b}} = \ln\frac{G^{b0}}{G^{b}} = \ln\frac{E^{b0}}{E^{b}} \tag{3-27}$$

where K^{b0}, G^{b0}, E^{b0} and K^{b}, G^{b}, E^{b} are the bulk, shear and Young's modulus of the undamaged and damaged bonds, respectively.

Damage locus:

Damage locus is defined as an energy threshold

$$F^d = \frac{1}{2}\sigma_{ij}^b \varepsilon_{ij}^b - r^b(s) \tag{3-28}$$

where r^b is the value of energy threshold that depends on suction *s*

$$r^b(s) = r^b(0) + r_{0s}^b \cdot s \tag{3-29}$$

where $r^b(0)$ = damage threshold at zero suction (fully saturated)

r_{0s}^b = parameter defining the change rate of damage locus with suction.

Damage rule:

Damage rule gives the evolution of damage strain $d\varepsilon_{kl}^d$ with damage variable *L*. This relation is constrained by the evolution of bond elastic modulus and takes the form

$$d\varepsilon_{kl}^d = \varepsilon_{ij}^b dL \tag{3-30}$$

Damage evolution law:

It defines the evolution of damage locus r^b with damage variable *L*. A simple linear expression is considered

$$r^b = r_0^b + r_1^b L \tag{3-31}$$

where r_0^b = value of energy threshold at which damage starts

r_1^b = parameter defining the evolution rate of damage locus, as a function of suction

$$r_1^b = r_{10}^b + r_{11}^b \cdot s \tag{3-32}$$

with parameters r_{10}^b and r_{11}^b.

Rate dependency:

Rate dependency is introduced by a delayed micro-cracking and uses the visco-damage formalism. The damage variable is expressed as a function of distance between the current bond stress point and the infinitely slow damage locus:

$$dL = \frac{dt}{\eta^b} \left\langle F^d \right\rangle \tag{3-33}$$

where η^b is the damage viscosity of bonds.

Infinitely slow damage locus takes the form

$$\overline{F}^d = F^d - \frac{\eta^b}{dt} dL \leq 0 \tag{3-34}$$

3.1.4 Coupling model for the composite material

The behaviour of the composite material is determined by coupling the responses of both clay matrix and bonds under the restrictions that a) the local strains ε_{ij} and ε_{ij}^b must be compatible with the external strains ε_{ij}^M, and b) the local stresses σ_{ij}^M and σ_{ij}^b must be in equilibrium with the external stresses σ_{ij}:

$$d\varepsilon_{ij}^M = d\varepsilon_{ij} + d\varepsilon_{ij}^b \tag{3-35}$$

$$\sigma_{ij} = (1+\chi)\sigma_{ij}^M + \chi\sigma_{ij}^b \tag{3-36}$$

with

$$\chi = \frac{\varepsilon_v^b}{\varepsilon_v} = \frac{\varepsilon_q^b}{\varepsilon_q} = \chi_0 \cdot \exp\left(-L/2\right) \tag{3-37}$$

where χ_0 is a coupling parameter defining the relative importance of the bond- and matrix-behaviour in the overall response of the composite material. The structure parameter χ decreases as damage evolves inside the bonds. In case of fully damage ($L \rightarrow \infty$), the rock behaves like the de-structured soil (clay matrix).

3.1.5 Parameters

In total, there are 18 independent parameters in the damage-elastoplastic model. Most parameter values for the Opalinus clay and the Callovo-Oxfordian argillite are given in /VAU 03/04/. For the scoping calculations, some of them were taken directly from the literature whereas the others were determined in GRS' laboratory tests for the Opalinus

clay. All parameters are represented in Table 3. Note, that some parameters could not be determined with appropriate accuracy due to a lack of test data.

Table 3 Parameters of the damage-elastoplastic model for the Opalinus clay

Symbol	Unit	Equation	Value
E^M	MPa	(3-16)	2500
ν^M	-	(3-16)	0.28
K_s^M	MPa	(3-16)	30000
m^M	-	(3-18)	7
$R_c^M(0)$	MPa	(3-20)	7
r^M	-	(3-20)	2
β^M	MPa^{-1}	(3-20)	0.003
ξ_r^M	-	(3-22)	0.02
α^M	-	(3-22)	0.3
η^M	MPa·s	(3-24)	10^6
E^b	MPa	(3-26)	7000
ν^b	-	(3-26)	0.28
$r^b(0)$	MPa	(3-29)	0.01
r_{0s}^b	-	(3-29)	0.0001
r_{10}^b	MPa	(3-31)	0.04
r_{11}^b	-	(3-31)	0.7
η^b	MPa·s	(3-33)	10^4
χ_0	-	(3-37)	0.38

The parameters of Hoek & Brown's yield function (the uniaxial compressive strength R_c^M, the tensile strength p_t^M and the parameter m^M) were determined on the basis of the peak strengths perpendicular to, parallel to and along the bedding plane /BOC 01/ that were obtained in triaxial tests on Opalinus samples. Figure 3.2 compares Hoek & Brown's model curves with the mean strength curves estimated from the lab tests. The Opalinus clay exhibits significant strength anisotropy, which however, is not yet included in the damage-elastoplastic model. Therefore an isotropic strength must be assumed for the actual modelling. The parameters of the strength curve parallel to the bedding were employed in the scoping calculations.

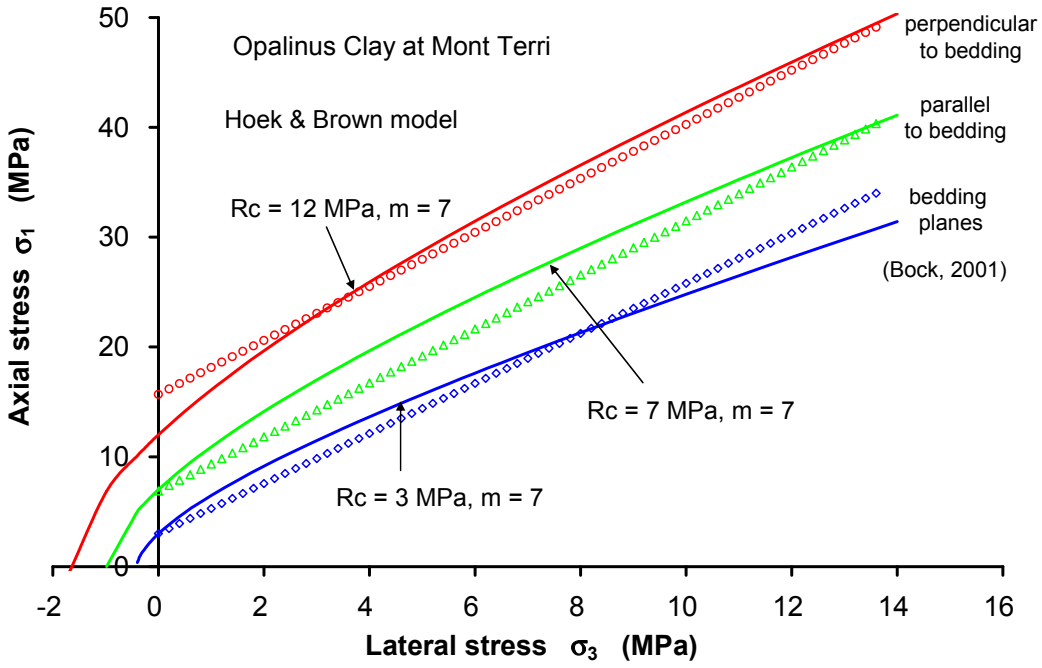

Figure 3.2 Anisotropic yield strength of the Opalinus clay

Stiffness and strength of clays increase with decreasing water content. Such effects are taken into account in the damage-elastoplastic model. Figure 3.3 shows the strength measured on samples of the Opalinus clay and the Callovo-Oxfordian argillite with different water content at confining pressures of 8 to 12 MPa. The model curves were obtained for a confining pressure of 10 MPa. The effect of water content on the strength is apparently well represented by the model.

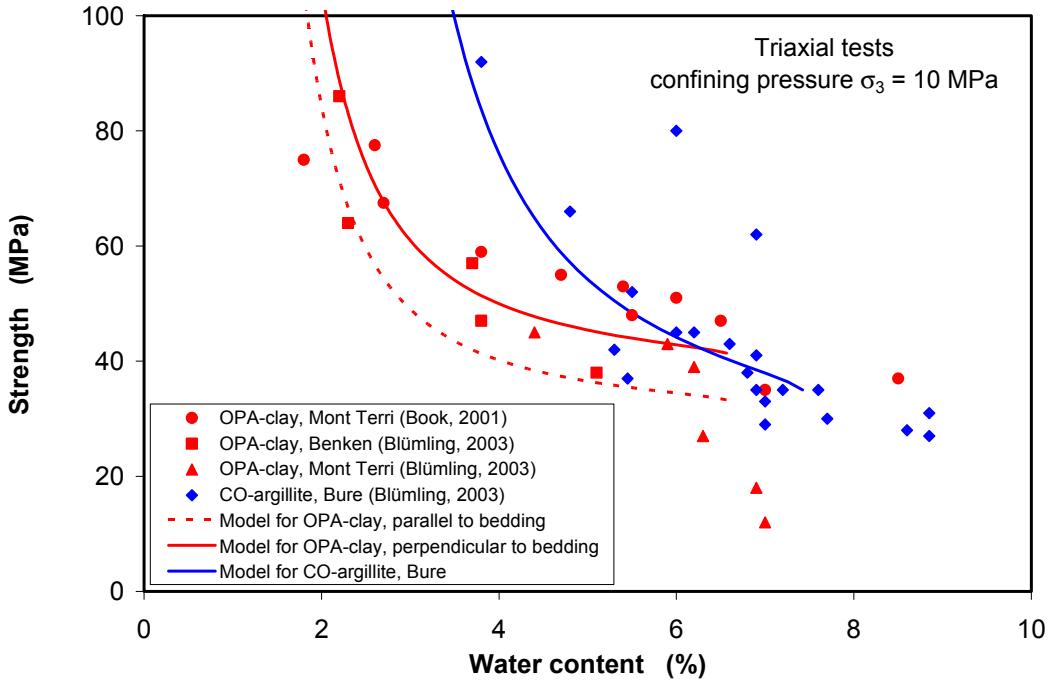

Figure 3.3 Dependency of the strength of the Opalinus clay and the Callovo-Oxfordian argillite on the water content

3.2 Hydraulic models

The hydraulic models and parameters for the Opalinus clay are listed in Table 4. Details about the models are given in /UPC 04/. Most of the parameter values are taken from the reports of the VE project /VE 02/, /FLO 02/, /MUN 03/ and /ZHA 05/. Figure 3.4 shows the water retention curve in comparison with the test results obtained by UPC /MUN 03/ and GRS /ZHA 05/. The permeability decreases with decreasing porosity, as shown in Figure 3.5. It is to be noted that the permeability-porosity relationship

$$k = k_o \frac{\phi^3}{(1-\phi^2)} \frac{(1-\phi_o)^2}{\phi_o^3} \tag{3-38}$$

may not be directly applied for permeability changes induced by fracturing. Gens et al. /GEN 07/ added a part of damage-induced porosity change by

$$\phi' = \phi + c_b \sqrt{D} \tag{3-39}$$

where c_b is a parameter. This improved permeability-porosity model will be examined by UPC in the frame of the running EC project TIMODAZ /TIM 06/.

Table 4 Hydraulic constitutive laws and parameters for the Opalinus clay

Law	Equation	Parameter
Darcy's law for advective flux of liquid and gas	$\mathbf{q}_\alpha = -\mathbf{K}_\alpha (\nabla P_\alpha - \rho_\alpha \mathbf{g})$ $\mathbf{K}_\alpha = \mathbf{k}\, k_{r\alpha} / \mu_\alpha$ α = *l* for liquid, α = *g* for gas	$\boldsymbol{k}$ = permeability tensor $k_{r\alpha}$ = relative permeability μ_α = dynamic viscosity
Intrinsic permeability	$\mathbf{k} = \mathbf{k}_0 \frac{\phi^3}{(1-\phi)^2} \frac{(1-\phi_0)^2}{\phi_0^3}$	$\boldsymbol{k}_o = k_o = 2\cdot10^{-20}$ m^2 ϕ = porosity, ϕ_o = 0.16
Relative permeability	$k_{rl} = A \cdot S_e^B, \quad k_{rg} = 1 - k_{rl}$ or $k_{rl} = \sqrt{S_e}\left[1 - \left(1 - S_e^{1/\lambda}\right)^\lambda\right]^2$	A = 1, B = 5 λ = 0.6
Saturation of liquid and gas	$S_e = \frac{S_l - S_{lr}}{S_{ls} - S_{lr}}$ $S_g = 1 - S_l$	S_{lr} = residual saturation = 0.01 S_{lr} = maximum saturation = 1 S_l = actual saturation S_e = effective saturation
Suction / saturation – relationship	$S_e = \left[1 + \left(\frac{s}{P_0}\right)^{1/(1-\beta)}\right]^{-\beta}$ s = suction (= $P_g - P_l$)	P_o =12 MPa, ß = 0.3 (averaged) P_o = 5 MPa, ß = 0.3 (drying path) P_o = 20MPa, ß = 0.3(wetting path)
Fick's law for vapour non-advective flux	$\mathbf{i}_g^w = -\mathbf{D}_g^w \nabla \omega_g^w$ $= -(\phi\ \rho_g\, S_g \tau\, \mathbf{D}_m^w\ \mathbf{I}) \nabla \omega_g^w$	$D_m^w = 5.9\cdot10^{-12} \cdot \frac{(273.15+T)^{2.3}}{P_g}$ m^2/s τ = tortuosity = 0.8
Psychrometric law for vapour mass per unit gas volume	$\theta_g^w = (\theta_g^w)^0 \exp\left[\frac{-(P_g - P_l) M_w}{R(273.15+T)\rho_l}\right]$	M_w = molecular mass of water = 0.018 kg/mol R = gas constant =8.314 J/(molK)
Henry's law for solubility of air in water	$\omega_l^a = \frac{P_a}{H} \frac{M_a}{M_w}$	M_a = molecular mass of air = 0.02895 kg/mol H = 10000 MPa
Liquid density	$\frac{\rho_l}{\rho_{lo}} = 1 + \beta(P_l - P_{lo}) + \alpha T$	ρ_{lo} = 1000 kg/m^3, α = -2.0·10^{-4} K^{-1} ß = 4.5·10^{-4} MPa^{-1}, P_{lo} = 0.1 MPa
Liquid viscosity	$\mu_l = A \exp\left(\frac{B}{273.15 + T}\right)$	A = 2.1·10^{-12} MPa s B = 1808.5 K
Ideal gas law	$P_g = \frac{\rho_g}{m} TR$	m = 28.966 kg/kmol for air m = 18.016 kg/kmol for vapour
Gas viscosity	$\mu_g = A \exp\left(\frac{B}{273.15 + T}\right)$	A = 1.48·10^{-12} MPa s B = 119.4 K

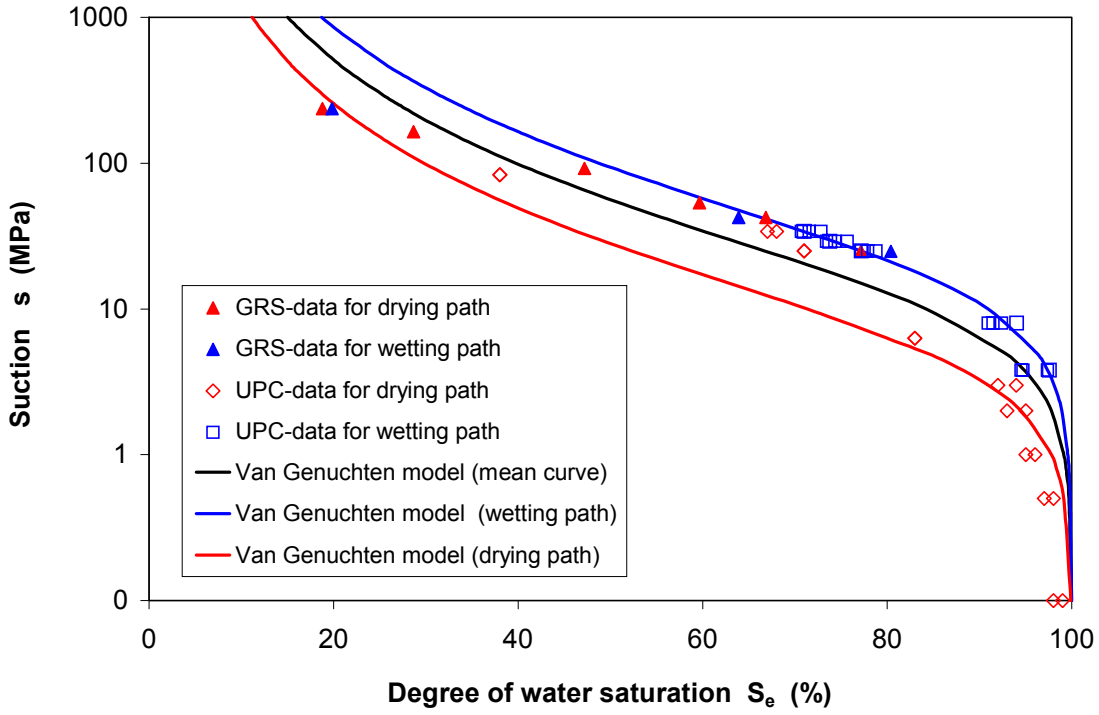

Figure 3.4 Water retention curves of the Opalinus clay

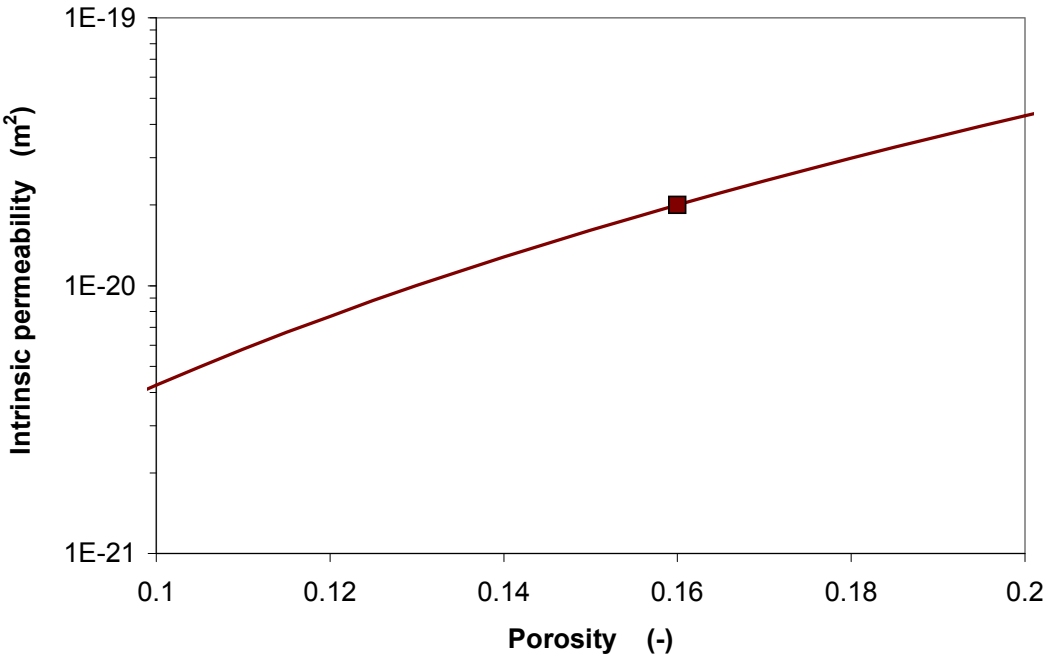

Figure 3.5 Intrinsic permeability as a function of porosity

In Figure 3.6 the gas permeability of the samples from the Callovo-Oxfordian argillite as measured by GRS /ZHA 04/ and the mathematical models describing the relative permeability-saturation relations for gas and water are compared. Apparently, there is a significant discrepancy between the model $k_{rl} = S_e^5$ and the test data. Generally, mechanisms of water and gas flow in indurated clays are not well understood, yet. More data are required to develop an adequate model for two-phase flow of water and gas in clay.

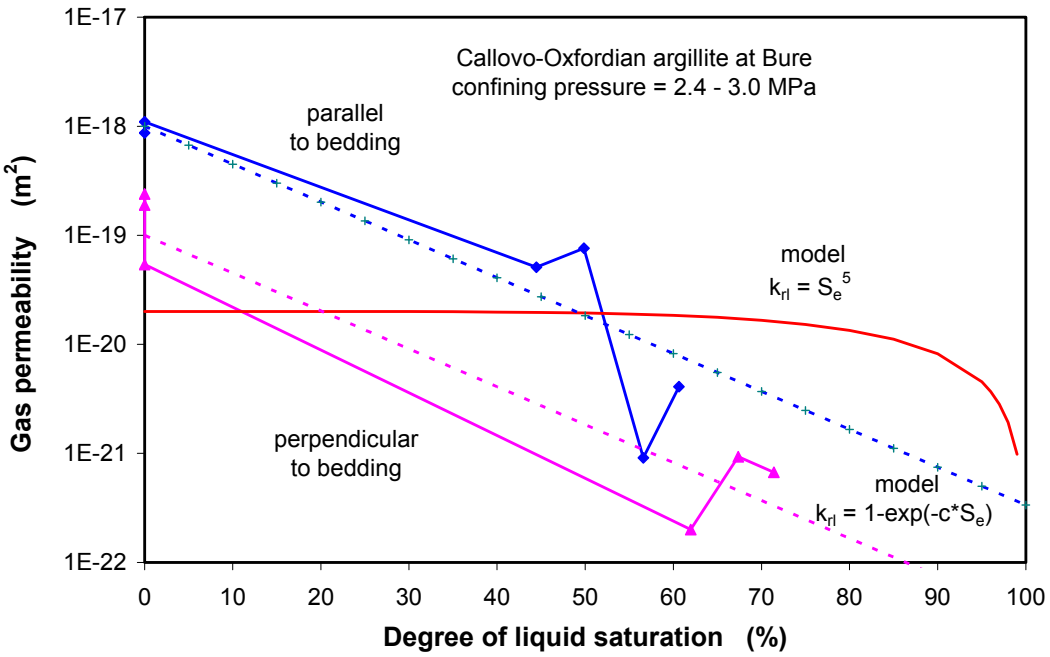

Figure 3.6 Gas permeability of the Callovo-Oxfordian argillite: comparison between the measured data and mathematical models

3.3 Test design

Originally, a large-scale damage-sealing test was proposed to be conducted on a hollow cylindrical sample with a central borehole. The sample should be extracted from the Opalinus clay at the Mont-Terri-URL and prepared to a size of 600 mm length, 55 mm inner diameter and 280 mm outer diameter. For the test, two concepts were proposed.

3.3.1 Test concept 1

Figure 3.7 shows the principle of test concept 1. The large hollow sample of D=280mm/ d=55mm/L=600mm is sealed with an inner and an outer rubber jacket. The pressure/stress exerted from the inner and outer pressure chamber on the sample will be called inner and outer stress, respectively, in the following. The test procedure was designed in the following steps:

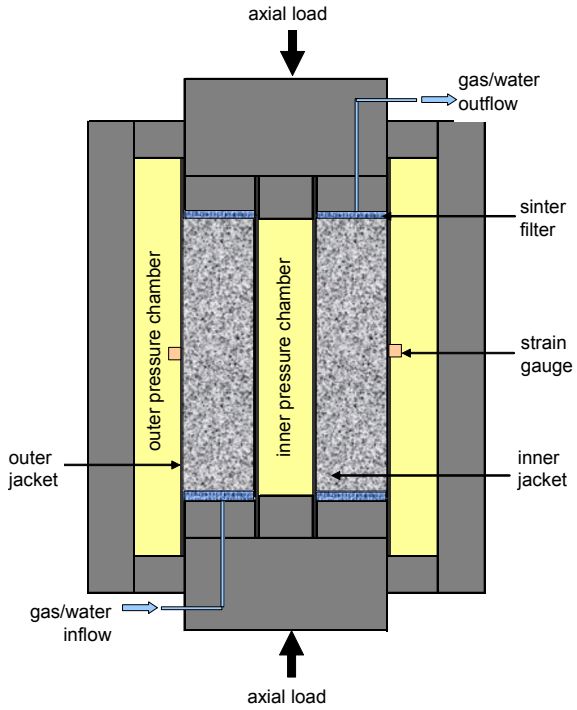

Figure 3.7 Principle of test concept 1

1. The sample is isotropically loaded by increasing the inner and outer confining stress up to 2.5 MPa. The inner stress in the borehole simulates the backfill support which is kept constant during the whole test.

2. Axial and outer radial stress will be increased to create an EDZ around the borehole. In order to ensure EDZ-like conditions throughout the whole sample, the loading process is considered to be performed in the following three steps: (1) increase of the axial and outer radial stress up to a high level of 30 MPa for generating a relatively large extent of the EDZ around the borehole, (2) reduction of the outer radial stress to 7.5 MPa for producing high deviatoric stresses and thus more damage in the whole sample, and (3) reduction of the axial load to 7.5 MPa. The final stress state, namely the inner stress of 2.5 MPa on the borehole wall and

the axial and outer radial confining stress of 7.5 MPa, should be representative for the conditions in the EDZ around drifts in the Mont-Terri-URL. It is to be pointed out that the high intensity and the large extent of the EDZ make it easy to observe coupled hydro-mechanical processes.

3. Under the constant load conditions, dry nitrogen gas is injected at the bottom face of the sample at a pressure of 1 MPa in order to detect a possible reduction of the gas permeability with time due to the impact of the applied external load. On the other hand, the dry gas inflow may displace the pore-water in large connected pores and the region near such pathways may be de-saturated due to the suction effect. Therefore, the ventilation effect on the development of the EDZ may be observable in the gas injection phase.

4. Following the gas injection, synthetic formation water will be injected at the bottom of the sample at a pressure of 2 MPa in order to simulate water flow into the EDZ and to observe the evolution of the water permeability. In this phase, the previously desaturated sample will be re-saturated again. After that, water outflow will be recorded to determine the water permeability. Because of possible compaction of the pores by creep and swelling of clay minerals during the re-saturation phase, a reduction of the water permeability with time can be expected.

5. Finally, a second gas injection will be carried out at controlled inflow rate in the range of 0.01 to 0.1 ml/min to simulate possible gas generation in repositories. During the gas injection, gas pressure may rise, depending on the degree of self-sealing of the damaged sample and the gas injection rate as well as the length of the pathways. Because the inflow rates in the laboratory may be much higher than those due to the much slower gas generation in repositories, the gas migration through the sample may differ from that in a real situation. In the test gas flow and gas pressure are measured at the inlet and the outlet of the sample to determine the gas entry and break-through pressure as well as the gas permeability after gas entering / breaking through. Comparing the gas permeability measured in this phase with that determined in the first gas injection phase may lead to a conclusion about the self-sealing potential of the EDZ.

3.3.2 Test concept 2

Because of the long hydraulic pathways through the sample, the conduction of test concept 1 may take an unacceptable long time for gaining reasonable results.

Therefore, another test concept is proposed as an alternative. Figure 3.8 shows the test principle. The hollow sample of D=260mm/d=55mm/L=600mm is sealed on the outside with a rubber jacket. The borehole is open during the mechanical loading phase. The borehole convergence will be measured at four locations, each in different horizontal directions by a dilatometer. After mechanical loading to create the EDZ, the sample will be unloaded and the outer jacket will be removed to identify possible damage on the sample surfaces visually. After that, the jacket will be applied again in such a way that a gap remains between borehole and sample. This gap will be backfilled with sand. The following hydraulic tests will be performed by injecting gas into the backfilled borehole and, subsequently, by injecting the backfilled outer gap with water. Because of the shorter pathways in radial direction, the test duration after concept 2 will be much shorter than that after concept 1. The test procedure of concept 2 is as follows:

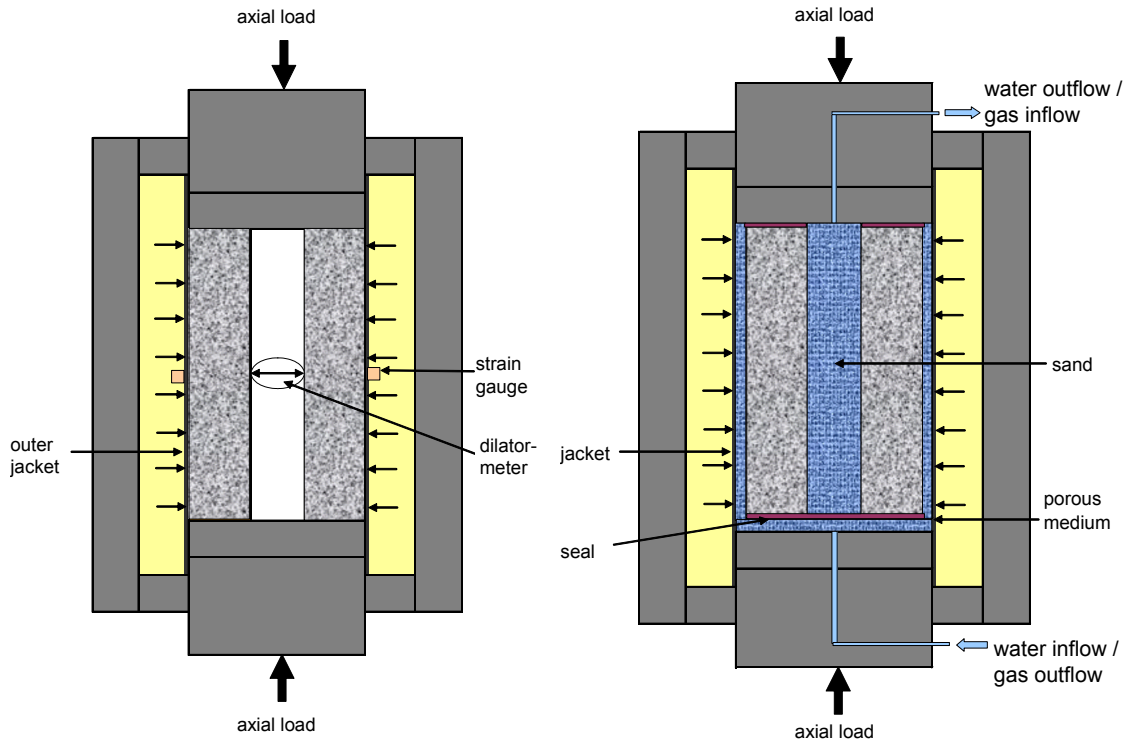

a. EDZ – generation

b. backfilling and gas/water injection

Figure 3.8 Principle of test concept 2

1. The hollow sample is loaded by increasing the axial and outer radial stress up to a high level of 30 MPa. Because the borehole is not supported, high deviatoric stresses will create a damaged zone around the borehole. To increase the intensity and extent of this EDZ, the radial stress will be reduced to 7.5 MPa, causing a

higher deviatoric stress distribution in the whole sample. Then, the axial load is reduced to 7.5 MPa. Finally, the damaged sample will be completely unloaded. After checking the damage on the surfaces, the borehole and the outer gap between sample and jacket will be backfilled with sand. It is possible to install pressure sensors in the backfilled borehole to monitor the backfill supporting stress. The backfilled sample will be reloaded again to the axial and outer radial confining stress of 7.5 MPa.

2. Under constant load conditions established at the end of the previous test phase, dry nitrogen gas is injected into the backfilled borehole at a pressure of 0.5 to 1 MPa and the gas flow outwards to the outer gap will be measured, in order to determine the gas permeability.

3. Following the gas injection, synthetic formation water is injected into the backfilled outer gap at a pressure of 1 to 2 MPa, simulating flow of formation water into the EDZ. Water outflow from the sample into the inner backfilled borehole will be recorded for determination of the water permeability.

4. Finally, gas will be injected into the backfilled borehole with a controlled inflow rate of 0.01 to 0.1 ml/min to simulate gas generation and to examine the gas entry and break-through pressure as well as the gas permeability after gas break-through.

3.4 Scoping calculations

Scoping calculations of the envisaged tests were carried out by solving the set of balance equations of energy, solid mass, water mass, air mass and stress equilibrium. The major assumptions are

- The mechanical behaviour of the Opalinus clay is described by the damage-elastoplastic model of Vaunat et al /VAU 03/.
- Water transport includes liquid water advection dominated by Darcy's law and vapour diffusion in the pore air (Fick's law). The liquid/gas phase changes are represented by the psychrometric law.
- Flow of dry air due to an air pressure gradient (Darcy's law) and dissolution of air in the liquid phase (Henry's law) are considered.
- The properties of the test sample are assumed to be homogeneous and isotropic.

3.4.1 Boundary conditions

Model calculations according to the two test concepts were performed using a 2D axisymmetric model for a sample geometry of D=260mm/d=55mm/L=600mm, as shown in Figure 3.9. Homogeneous and isotropic properties were assumed in the calculations of both tests. Because the samples were more or less de-saturated during sampling, storage and preparation, an initial state of 99% saturation with gas was assumed, corresponding to a suction of 1 MPa. The test temperature was kept at 20°C in the model. Modelling steps corresponding to the test phases described above and the referring boundary conditions are summarized in Tables 5 and 6 for both test concepts, respectively. Note that the backfilling of the borehole and the outer gap between the sample and the jacket according to concept 2 was not considered in the model.

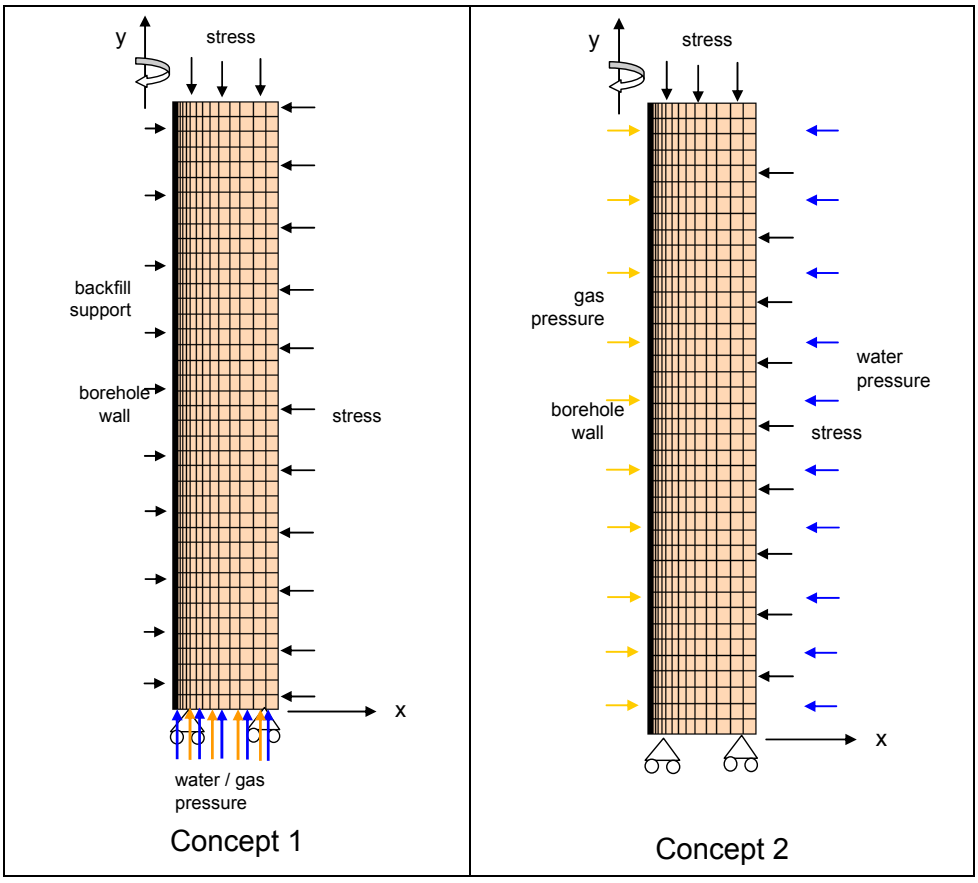

Figure 3.9 Model geometry and boundary conditions for two test concepts

Table 5 Modelling steps and boundary conditions for test concept 1

Step 0:	t = 0, application of initial conditions porosity ϕ = 15%, temperature T = 20°C, suction s = 1 MPa, gas pressure P_g = 0.1 MPa, isotropic stress $\sigma_z = \sigma_x = \sigma_y$ = 2.5 MPa
Step 1:	t = 0 to 0.83 hour, application of external confining stress constant backfill support $\sigma_{r\text{-}in}$ = 2.5 MPa, simultaneous increase of axial and radial stresses σ_a and $\sigma_{r\text{-}out}$ up to 30 MPa each by applying strain rates of $du_a/dt = 3 \cdot 10^{-7}$ m/s and $du_r/dt = 1 \cdot 10^{-7}$ m/s
Step 2:	t = 0.83 to 2.5 hour, reduction of the outer radial stress to 7.5 MPa by $du_r/dt = 1 \cdot 10^{-7}$ m/s
Step 3:	t = 2.5 to 5.9 hour, reduction of the axial stress to 7.5 MPa by $du_a/dt = 3 \cdot 10^{-7}$ m/s
Step 4:	t = 5.9 to 2000 hour, gas injection at the bottom of the sample at a pressure of P_g = 1 MPa under $\sigma_{r\text{-}in}$ = 2.5 MPa, $\sigma_a = \sigma_{r\text{-}out}$ = 7.5 MPa, atmospheric pressure P_g = 0.1 MPa applied on top of the sample
Step 5:	t = 2000 to 6000 hour, water injection at the bottom of the sample at a pressure of P_l = 2 MPa, atmospheric water pressure P_l = 0.1 MPa on the top of the sample
Step 6:	t = 6000 to 10000 hour, gas injection at the bottom of the sample with a constant inflow rate of $1 \cdot 10^{-9}$ or $1 \cdot 10^{-8}$ kg/s (corresponding to pumping rates of 0.01 to 0.1 ml/min) at atmospheric pressure of P_g = 0.1 MPa on top of the sample

Table 6 Modelling steps and boundary conditions for test concept 2

Step 0:	t = 0, application of initial conditions porosity ϕ = 15%, temperature T = 20°C, suction s = 1 MPa, gas pressure P_g = 0.1 MPa, isotropic stress $\sigma_z = \sigma_x = \sigma_y$ = 2.5 MPa

Step 1:	t = 0 to 1 hour, application of external confining stress no backfill support $\sigma_{r\text{-}in}$ = 0 MPa, simultaneouse increase of axial and radial stresses σ_a and $\sigma_{r\text{-}out}$ up to 30 MPa each by applying strain rates of $du_a/d\,t = 3 \cdot 10^{-7}$ m/s and $du_r/dt = 1 \cdot 10^{-7}$ m/s
Step 2:	t = 1 to 2.6 hour, reduction of the outer radial stress to 7.5 MPa by $du_r/dt = 1 \cdot 10^{-7}$ m/s
Step 3:	t = 2.6 to 6 hour, reduction of the axial stress to 7.5 MPa by $du_a/dt = 3 \cdot 10^{-7}$ m/s
Step 4:	t = 6 to 1000 hour, gas injection into the backfilled borehole at a pressure of P_g = 0.5 or 1 MPa under $\sigma_{r\text{-}in}$= 0 MPa, $\sigma_a = \sigma_{r\text{-}out}$ =7.5 MPa, atmospheric pressure P_g = 0.1 MPa on the outer peripheral surface of the sample. No backfill in the borehole or in the gap between the sample and the jacket considered in the model
Step 5:	t = 1000 to 3000 hour, water injection at the external peripheral surface of the sample at a pressure of P_l = 1 MPa, atmospheric water pressure P_l = 0.1 MPa in the backfilled borehole
Step 6:	t = 3000 to 6000 hour, gas injection into the borehole again with a constant inflow rate of $1 \cdot 10^{-9}$ or $1 \cdot 10^{-8}$ kg/s at atmospheric pressure of P_g = 0.1 MPa on the external peripheral surface

3.4.2 Modelling results

Step 1-3: EDZ - Generation

Figure 3.10 and 3.11 illustrate the response of the clay samples to the mechanical loading for both test concepts. Because of almost the same initial / boundary conditions and loading procedures in both tests, the resulting hydro-mechanical effects in the samples are quite similar. The first load with increasing the axial and outer radial stress

up to 30 MPa causes an axial compression and a radial deformation towards the borehole (negative value), as shown in Figure 3.10b and 3.11b. While the outer region remains intact during loading, indicated by the reduction of the porosity (Fig. 3.10c, 3.11c), the inner region of 15 - 20 mm thickness near the borehole wall is damaged due to the highly concentrated deviatoric stress, indicated by the increase of the porosity. This dilatancy zone is here defined as EDZ. The EDZ extends to about 1/3 of the borehole diameter or 1/5 of the thickness of the sample ring. In the second load-step, the outer radial stress is reduced to 7.5 MPa and thus a high deviatoric stress is built up in the whole sample, resulting in an increase of the porosity. The following reduction of the axial stress to the same level as the radial stress causes an additional increase of the porosity mainly due to the elastic recovery. In addition to the mechanical behaviour, the load causes also significant changes of the pore-water pressure (Fig. 3.10d, 3.11d). In the more compacted outer region, the pore-water pressure is higher. After reducing the axial and outer radial stress to 7.5 MPa, the pore-water pressure decreases down to zero or even to negative levels which is caused by the increase of the pore spaces.

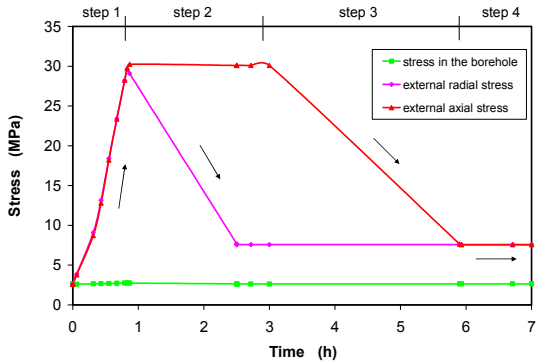

a. axial, outer / inner radial stress

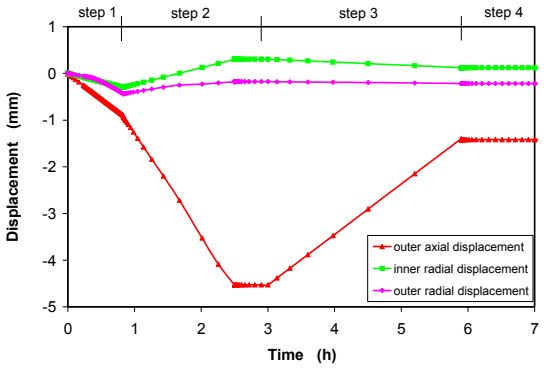

b. axial, outer / inner radial displacement

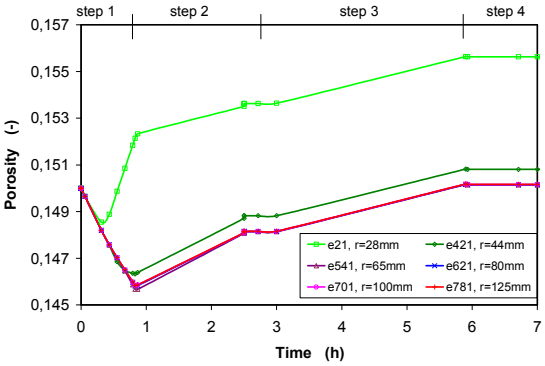

c. porosity

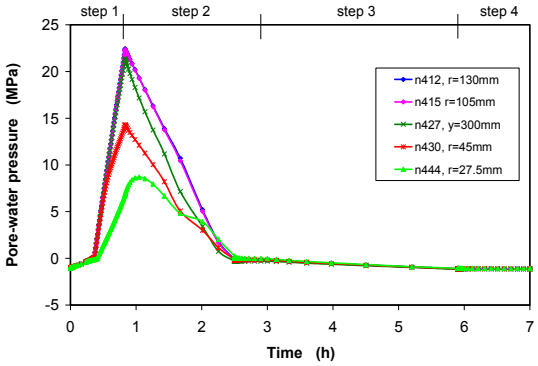

d. pore-water pressure

Figure 3.10 Response of the sample to the mechanical loading in test concept 1

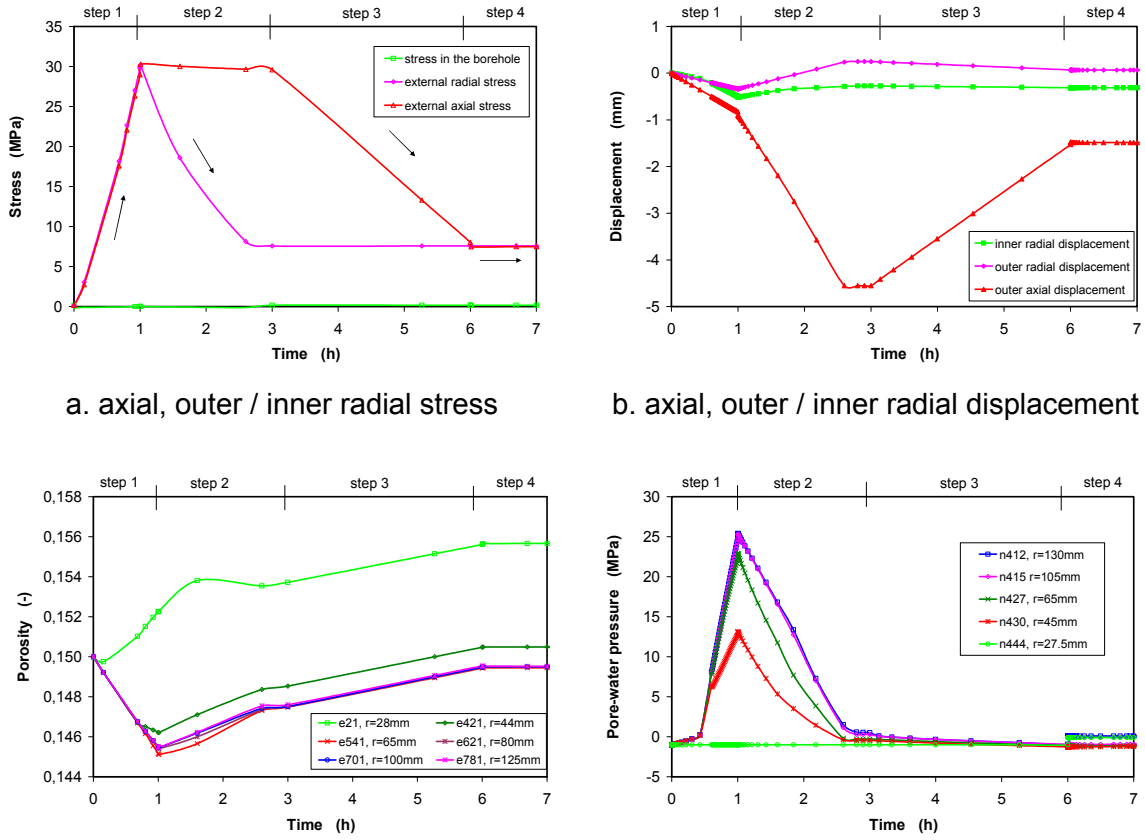

a. axial, outer / inner radial stress

b. axial, outer / inner radial displacement

c. porosity

d. pore-water pressure

Figure 3.11 Response of the sample to the mechanical loading in test concept 2

Step 4: Gas injection at constant pressure

Figure 3.12 and 3.13 show the modelling results for the gas injection at the bottom of the sample at a pressure of 1 MPa according to test concept 1 and of the gas injection to the inner peripheral surface at 0.5 MPa according to concept 2, respectively. Whereas the gas pressure in sample 1 is still increasing after 2000 hours, a steady state of the gas pressure in sample 2 is reached after about 200 hours. Gas outflow at the end of the injection phase amounts to $3 \cdot 10^{-16}$ kg/s for concept 1, which is one order of magnitude lower than the outflow of $3 \cdot 10^{-15}$ kg/s calculated for concept 2. The back-calculations yield a very low gas permeability of $1 \cdot 10^{-26}$ m^2 of the damaged samples. The low gas permeability is caused by the nearly full water saturation which does not allow gas flow through the pores. However, this modelling result is significantly differing from the values measured on the damaged clay samples (see chapter 2) and those

measured in the EDZ around drifts. The main reasons for this could be that: a) the mechanical constitutive model applied is not able to represent fracturing which is the dominating mechanism for the development of EDZ in indurated clays, or b) the permeability is not related to fractures but only weakly to porosity.

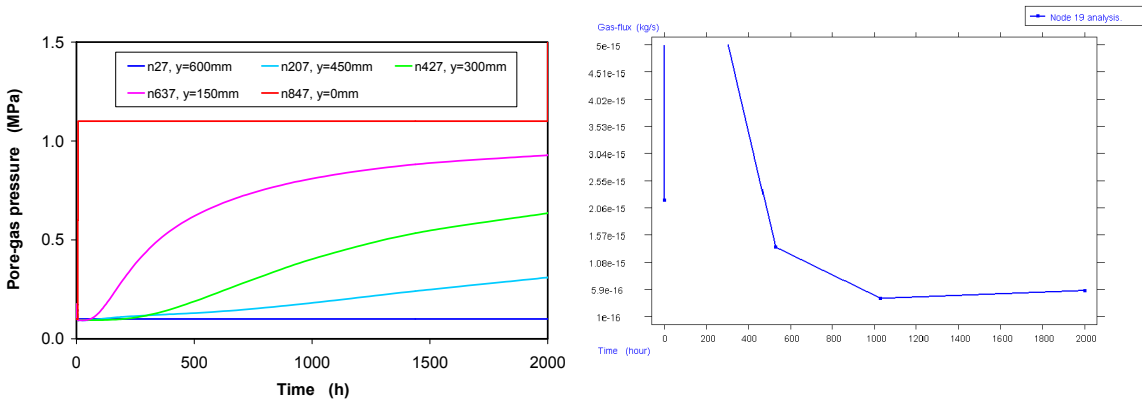

a. pore-gas pressure

b. gas outflow

Figure 3.12 Gas injection and outflow in test concept 1

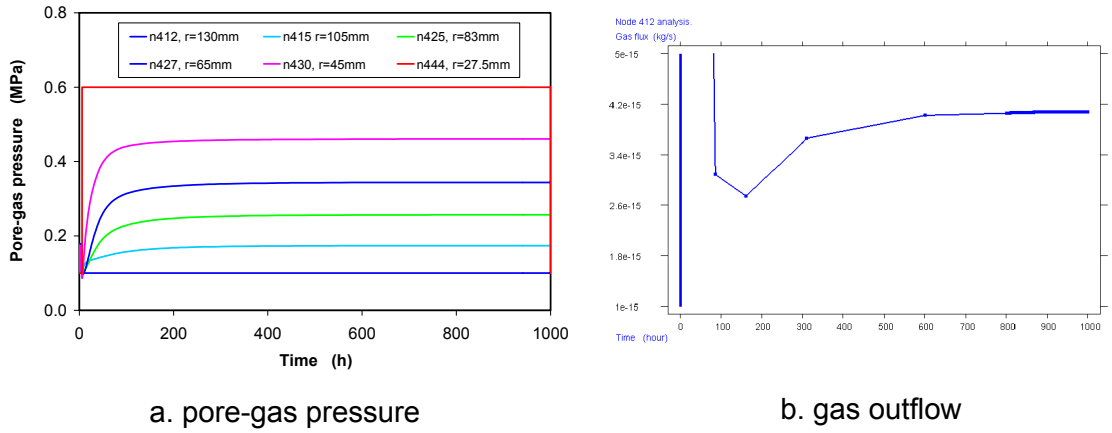

a. pore-gas pressure

b. gas outflow

Figure 3.13 Gas injection and outflow in test concept 2

Step 5: Water injection at constant pressure

Figure 3.14 and 3.15 illustrate the modelling results of the water injection into the bottom of the sample at a pressure of 2 MPa according to concept 1 and into the inner peripheral surface at 1 MPa according to concept 2, respectively. Whereas steady state water flow is reached after about 1500 hours in concept 1, the time required for steady state water flow in concept 2 is about 100 hours. The steady state water flux out

of the sample in concept 1 is $7 \cdot 10^{-11}$ kg/s, which is about one order of magnitude lower than the outflow in concept 2 amounting to $4 \cdot 10^{-10}$ kg/s. The back-calculations yield a water permeability of 10^{-22} m^2. This value is 2 orders of magnitude lower than that of 10^{-20} m^2 observed in the lab tests.

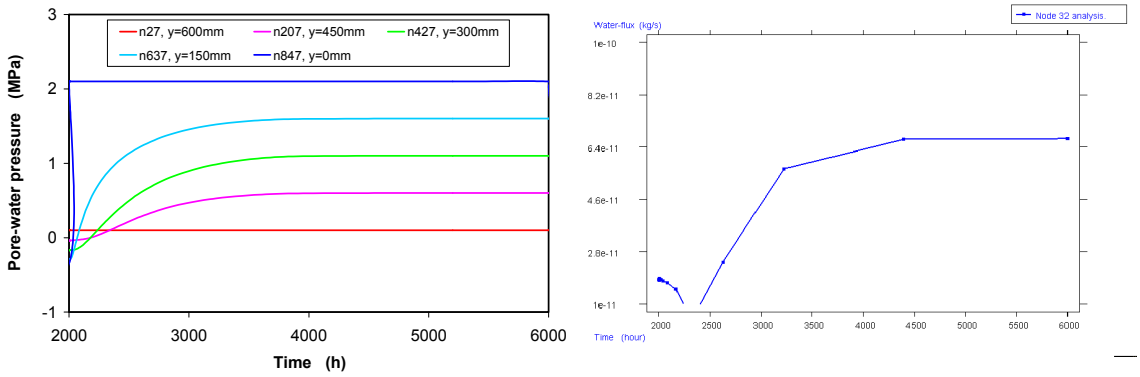

a. pore-water pressure

b. water outflow

Figure 3.14 Water injection and outflow in test concept 1

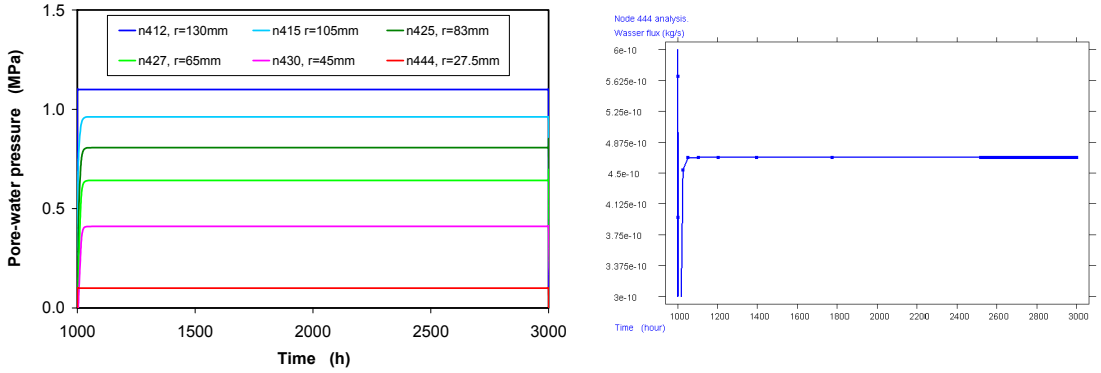

a. pore-water pressure

b. water outflow

Figure 3.15 Water injection and outflow in test concept 2

Step 6: Gas entry / break-through pressure

Gas entry and/or break-through pressure of the samples damaged and then re-sealed before is modelled for constant gas inflow rates of $1 \cdot 10^{-9}$ and $1 \cdot 10^{-8}$ kg/s (corresponding to pumping rates of 0.01 and 0.1 ml/min respectively). Figure 3.16 shows the development of the gas pressure at the inlet for both test concepts. It is obvious that the inlet gas pressure builds up rapidly and then remains constant. The higher the

inflow rate, the higher the gas pressure. Because the gas pressure in sample 1 is higher than the sum of the minimum confining stress of 2.5 MPa on the borehole wall and the tensile strength of 1 – 2 MPa, a high break-through pressure of about 4 MPa is calculated for the inflow rate of $1 \cdot 10^{-8}$ kg/s. After reaching this high pressure the calculation ceased. It is difficult from the modelling curves to distinguish between gas entry pressure and break-through pressure.

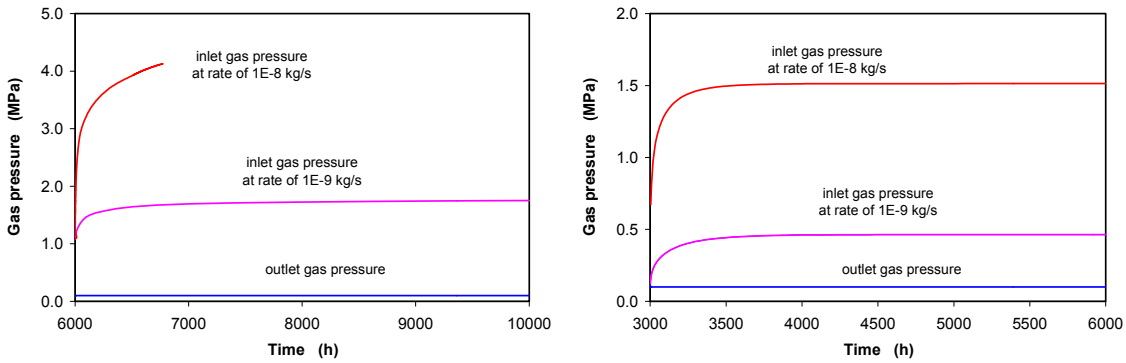

a. concept 1 b. concept 2

Figure 3.16 Build-up of gas pressure in clay sample

Remarks

It seems that some aspects dealing with damage and sealing of indurated clay are not sufficiently considered in the constitutive models used here which are among others:

- permeability changes induced by damage/fracturing,
- anisotropy of the permeability related to the major stress direction and the bedding plane as a further result of damage/fracturing, and
- sealing of fractures due to mechanical compaction and water resaturation.

In the framework of the EC-project TIMODAZ /TIM 06/, the permeability changes induced by damage and compaction will be determined for providing an improved database. Additionally, test concept 1 with some modifications will be realised and numerically modelled by the project partners of TIMODAZ using various models.

4 Summary

The self-sealing potential of the Callovo-Oxfordian argillite and the Opalinus clay was investigated on strongly damaged samples. Gas permeability as a function of the confining stress before and after water resaturation was measured. Not only normally-sized but also large-scale and cylindrical ring-shaped samples were tested. Each test lasted over a time period of 5 to 16 months. The experimental findings are:

- The permeability of the pre-damaged samples decreased significantly with a concurrent increase of the confining stress due to fracture closure. The permeability measured in radial direction on a hollow sample decreased from 10^{-15} m^2 at a low confining stress of 1 MPa to 10^{-21} m^2 at 28 MPa. The compression of the sample led to plastic closure of pre-existing fractures, leading to a significantly lower permeability after unloading. A similar permeability reduction with increasing confining stress was also observed in axial direction, parallel to the bedding plane. But, at low confining stresses below 10 MPa, the axial permeability parallel to the bedding was about one to two orders of magnitude higher than the radial one perpendicular to the bedding. The hydraulic anisotropy vanishes off with increasing the confining stress.

- The permeability of fractured clay rocks was dominated by the confining stress normal to the fracture plane. This was validated by gas permeability measurements on a large sample (D=260mm/L=616mm) with fractures oriented parallel to the sample axis. The increase of the lateral stress from 3 to 18 MPa at 19 MPa axial stress led to a decrease of axial permeability from 10^{-13} to 10^{-19} m^2.

- The permeability of damaged clay rocks decreased also with time due to the time-dependent compaction of pores and fractures. On the pre-damaged samples, a permeability reduction by a factor of 4 to 8 was observed over two months at a low confining stress of 1.5 MPa.

- The high swelling potential of the studied clay rocks led to the closure of fractures when water was injected into the sample. This was confirmed by a pronounced decrease of the gas permeability from 10^{-16} to 10^{-21} m^2 after water resaturation was reached.

- The re-sealed samples exhibited low permeability to gas and water of less than 10^{-20} m^2 as it is usually observed on undisturbed clay rocks. All these experimental

results provide evidence for the high self-sealing capacity of the studied clay rocks under the combined impact of reconsolidation and resaturation.

For the design of the envisaged damage-sealing tests on large hollow cylindrical samples, scoping calculations were performed using CODE-BRIGHT including a damage-elastoplastic model for indurated clay, which has been proposed by Vaunat et al /VAU 03/04/. This model assumes the clay to be a composite material of a clay matrix interlocked by bonds. The clay matrix behaves like a typical elastoplastic soil, while bonds behave like a typical quasi-brittle material represented by a damage-elastic law. The modelling results from UPC for the analysis of the EDZ development in clay rocks /VAU 03/04/, /GEN 07/, suggest the suitability of the model. However, some special aspects such as permeability changes due to damage, reconsolidation or resaturation as well as thermal impact on the long-term evolution and self-sealing of the EDZ are to be involved in the models for safety assessment of repositories in clay formations. Some of these issues will be investigated in the framework of the other running projects TIMODAZ /TIM 06/ and THM-TON /GRS 07/.

5 Acknowledgements

The work described in this report was funded by the German Federal Ministry of Economics and Technology (BMWi) under contract number 02E9834 and by the European Commission under contract number F16W-CT-2003-02389. The authors would like to thank for this support. The support from the French Agence Nationale Pour la Gestion de Déchets Radioactifs (ANDRA) for providing the testing material and the support from the Geotechnical Engineering Department of the Technical University of Catalonia in Barcelona (UPC) for helping with the modelling work are also gratefully acknowledged. Many thanks go also to all project partners involved in the NF-PRO-WP4.4 for the fruitful discussions during the project meetings. The review made by Dr. K.-P. Kröhn is acknowledged, too.

6 References

/AND 05/ ANDRA. 2005: DOSSIER 2005 Argile Synthesis – Evaluation of the feasibility of a geological repository in an argillaceous formation, Meuse/Haute-Marne site.

/BOC 01/ Bock, H. (2001): RA Experiment - Rock mechanics analyses and synthesis: Data Report on Rock Mechanics. Technical Report 2000-02.

/FLO 02/ Floria, E.; Sanz, F.J.; Garcia-Sineriz, J.L. (2002): Drying test: evaporation rate from core samples of “Opalinus clay” under controlled environmental conditions, VE-Deliverable 6.

/GEN 07/ Gens, A., Vaunat, J, Garitte, B. & Wileveau, Y. (2007): In-situ behaviour of a stiff layered clay subject to thermal loading: observations and interpretation. Geotechnique 57, No. 2, 207-228.

/GRG 06/ Grgic, D, Homand, F. & Hoxha, D. (2006): Short- and long-term constitutive model for porous rocks. EUROCK 2006 ISRM regional symposium Multiphysics coupling and long-term behaviour in rock mechanics, 9 – 12 May 2006, Liège, Belgium.

/GRS 07/ GRS’ Projekt (2007): Untersuchung der THM-Prozesse im Nahfeld von Endlagern in Tonformationen, FZK 02E10377.

/HOX 06/ Hoxha, D, Jiang, Z, Homand, F., Giraud, A., Su, K. & Wileveau, Y. (2006): Impact of THM constitutive behavior on the rock-mass response: case of HE-D experiment in Mont Terri Underground Rock Laboratory. EUROCK 2006 ISRM regional symposium Multiphysics coupling and long term behaviour in rock mechanics, 9 – 12 May 2006, Liège, Belgium.

/JIA 06/ Jia, Y., Duveau, G., Shao, J.F., Su, K. & Wileveau, Y. (2006): Thermo-hydro-mechanical modeling in unsaturated hard clay and application to nuclear waste storage. EUROCK 2006 ISRM regional symposium Multiphysics coupling and long term behaviour in rock mechanics, 9 – 12 May 2006, Liège, Belgium.

/MUN 03/ Munoz, J.J.; Lioret, A.; Alonso, E. (2003): Laboratory Report : Characterization of hydraulic properties under saturated and non saturated conditions, VE-Deliverable 4.

/PEA 03/ Pearson, F.J., Arcos, D., Bath, a., Boison, J.-y., Fernández, A.M., Gäbler, H.-E., Gaucher, E., Gautschi, A., Griffault, L., Hernán, P., Waber, H.N., 2003: Mont Terri Project – Geochemistry of Water in the Opalinus Clay Formation at the Mont Terri Rock Laboratory. No 5 – Bern 2003.

/SU 07/ Su, K. (2007): Synthesis of the MODEX-REP Project: Development and Validation of the Constitutive Hydro-mechanical Models for Callovo-Oxfordian Argillites. EC – 5th EURATOM framework programme, FIKW-CT-2000-00029, February 2007.

/TIM 06/ TIMODAZ (2006): Thermal Impact on the Damaged Zone Around a Radioactive Waste Disposal in Clay Host Rocks. EC-FP6-036449.

/UPC 04/ UPC (2004): CODE-BRIGHT, A 3-D program for thermo-hydro-mechanical analysis in geological media.

/VAU 03/ Vaunat, J.; Alonso, E.E.; Gens, A. (2003): Constitutive model of short and long term behaviour of the Meuse/Haute-Marne argillite. Deliverable 2&3 of the project MODEX-REP, FIKW-CT2000-00029.

/VAU 04/ Vaunat, J. & Gens, A. (2004): Aspects of modelling geotechnical problems in hard soils and soft argillaceous rocks. Proc. In. Symp. on Numerical Models in Geomechanics.

/VE 02/ VE (2002): Ventilation Experiment in Opalinus clay – „VE“ Experiment, VE Test Plan, Deliverable 3, EC contract FIKW-CT2001-00126.

/ZHA 04/ Zhang, C.L. & Rothfuchs, T. (2004): Experimental Study of Hydro-mechanical Behaviour of the Callovo-Oxford Argillites. Applied Clay Science 26 (2004) 325-336.

/ZHA 05/ Zhang, C.L., Rothfuchs, T., Su, K., Hoteit, N. (2005): Experimental Study of the Thermo-Hydro-Mechanical Behaviour of Indurated Clays. Physics and Chemistry of the Earth, Vol 32, 8-14, 2007, p. 957-965.

/ZHA 06/ Zhang, C.L., Wieczorek, K., Rothfuchs, T. (2006): Experimental study on damage and self-sealing of indurated clays, Poster presentation on the NF-PRO-Third Workshop, 14-16 Nov. 2006, Spain.

/ZHA 07a/ Zhang, C.L., Rothfuchs, T., Jockwer, N., Wieczorek et al. (2007a): Thermal Effects on the Opalinus Clay – A Joint Heating Experiment of ANDRA and GRS at the Mont Terri URL (HE-D Projekt), GRS-224, 2007.

/ZHA 07b/ Zhang, C.L. & Rothfuchs, T. (2007b): Moisture Effects on Argillaceous Rocks. 2nd International Conference of Mechanics of Unsaturated Soils (ed. by T. Schanz), Springer Proceedings in Physics 112, 2007, 319-326.

/ZHA 07c/ Zhang, C.L. & Rothfuchs, T. (2007c): Damage and Sealing of Clay Rocks Detected by Permeability Measurements. 3rd International Clay Meeting, Lille, Sept. 17-20, 2007.

7 List of Figures

8 List of Tables

Gesellschaft für Anlagen- und Reaktorsicherheit (GRS) mbH

Schwertnergasse 1
50667 Köln
Telefon +49 221 2068-0
Telefax +49 221 2068-888

Forschungsinstitute
85748 Garching b. München
Telefon +49 89 32004-0
Telefax +49 89 32004-300

Kurfürstendamm 200
10719 Berlin
Telefon +49 30 88589-0
Telefax +49 30 88589-111

Theodor-Heuss-Straße 4
38122 Braunschweig
Telefon +49 531 8012-0
Telefax +49 531 8012-200

www.grs.de

ISBN 978-3-939355-04-5